Towards high-performance dye-sensitized solar cells by utilizing reduced graphene oxide-based composites as potential alternatives to conventional electrodes: A review

Next Materials 6 (2025) 100477

Contents lists available at ScienceDirect

Next Materials

journal homepage: www.sciencedirect.com/journal/next-materials

Review article

Towards high-performance dye-sensitized solar cells by utilizing reduced graphene oxide-based composites as potential alternatives to conventional electrodes: A review

Edigar Muchuweni [a,*], Edwin T. Mombeshora [b,1], Cosmas M. Muiva [c], T. Stephen Sathiaraj [d], Abdullah Yildiz [e], Diego Pugliese [f]

[a] Department of Engineering and Physics, Bindura University of Science Education, Private Bag 1020, Bindura, Zimbabwe
[b] School of Chemical and Metallurgical Engineering, University of the Witwatersrand, WITS, Johannesburg 2050, South Africa
[c] Department of Physics and Astronomy, Botswana International University of Science and Technology, Private Bag 16, Palapye, Botswana
[d] Department of Physics and Computer Science, Wilfrid Laurier University, Waterloo N2L 3C5, Canada
[e] Department of Energy Systems Engineering, Ankara Yildirim Beyazit University, Ankara 06010, Turkey
[f] National Institute of Metrological Research (INRiM), Strada delle Cacce 91, Torino 10135, Italy

ARTICLE INFO

Keywords:
Dye-sensitized solar cell
TiO_2-free photoanode
Pt-free counter electrode
Reduced graphene oxide
Nanocomposite

ABSTRACT

Dye-sensitized solar cells (DSSCs) have recently emerged as one of the most promising new-generation photovoltaic devices due to their facile fabrication protocols, capacity to operate under diffuse light, and low-impact on the environment. However, their low power conversion efficiency (~15.2%) hinders practical applications. This is primarily owing to ineffective dyes, significant recombination at solid/liquid interfaces, and limitations of TiO_2, the conventional photoanode material, especially poor light harvesting and electron transport. Moreover, Pt, the traditional counter electrode material, is costly and unstable due to its scarcity and low corrosion resistance to I_3^-, respectively. This increases the device cost and shortens its lifespan. Inspired by this, current research interests have shifted their focus from traditional materials to low-cost alternatives, including metal oxides, metal chalcogenides and perovskites, which offer competitive photovoltaic performance. Nonetheless, these alternative materials exhibit relatively low electrical conductivity, which compromises device performance. Thus, to improve device efficiency and sustainability, these materials have recently been coupled with highly conductive and stable carbon nanomaterials, particularly graphene-based materials. Among them, reduced graphene oxide (rGO) has been more appealing due to its compatibility with low-cost solution processing. Therefore, this review highlights the recent advances in DSSC efficiency and sustainability made over the last five-years (2020–2024) by developing TiO_2-free photoanodes and Pt-free counter electrodes, in particular, by introducing rGO into metal oxides, metal chalcogenides and perovskites. Challenges and future directions for fabricating TiO_2- and Pt-free DSSCs are discussed to close the gap between emerging nanomaterials and their traditional counterparts, thereby setting the stage for commercialization.

1. Introduction

Almost 80% of the daily global energy consumption is generated from fossil fuels, such as coal, natural gas and oil [1–6]. However, these traditional energy sources will soon fail to meet the increasing energy demand due to their non-renewable nature, which is causing their rapid depletion. Also, the continuous usage of fossil fuels is becoming a serious threat to the well-being of humans and the environment since fossil fuels release greenhouse gases that cause undesirable effects, such as pollution, global warming, acid rain and climate change [7–12]. Consequently, renewable energy sources, such as geothermal [13,14], biomass [15,16], wave [17,18], wind [19,20], solar [21,22] and hydropower [23,24], have emerged as potential solutions to resolve the global energy crisis. Among these, solar energy has gained intensive research

* Corresponding author.
E-mail addresses: emuchuweni@buse.ac.zw (E. Muchuweni), edwin.mombeshora@wits.ac.za (E.T. Mombeshora), muivac@biust.ac.bw (C.M. Muiva), tsathiaraj@wlu.ca (T.S. Sathiaraj), abdullah.yildiz@aybu.edu.tr (A. Yildiz), d.pugliese@inrim.it (D. Pugliese).
[1] Permanent address: Department of Chemistry, University of Pretoria, Private Bag X20, Hatfield 0028, Pretoria, South Africa.

https://doi.org/10.1016/j.nxmate.2024.100477
Received 25 October 2024; Received in revised form 16 December 2024; Accepted 24 December 2024
Available online 4 January 2025

attention owing to its low-cost due to the natural abundance of free sunlight, and low impact on the environment due to the absence of carbon emissions.

Meanwhile, dye-sensitized solar cells (DSSCs), one of the new-generation photovoltaic devices, have recently emerged as a promising renewable energy technology for converting solar energy into electricity due to their simple fabrication protocols, diverse designs and orientation flexibility, low-costs, flexibility and capability to function even under diffuse light [25–30]. DSSCs were initially conceptualized in the late 1980s [31], and they made a considerable breakthrough in 1991 when Grätzel and O'Regan developed a high-performing DSSC with a power conversion efficiency (PCE) of ~8% using a mesoporous TiO_2 photoanode, a Ru(II) pyridyl complex dye, and an I^-/I_3^- redox electrolyte [32]. This device marked a substantial shift from traditional p-n junction solar cells by utilizing photoinduced electron injection into TiO_2 photoanodes of a dye-sensitized system. Subsequent research efforts have significantly increased device efficiency, stability and scalability through innovations in dyes, electrodes, and electrolytes [33–35]. In particular, the development of Ru-based dyes, D-π-A structured organic dyes, and porphyrin dyes has been central to improving visible light absorption and exciton dissociation [36]. Advances in photoanodes, especially those made from TiO_2 nanostructures, have been key to enhancing visible light harvesting and electron transport [37]. The development of high-performance counter electrodes, particularly those using Pt or carbon nanomaterials, has increased charge collection efficiency [38]. Innovations in liquid and quasi-solid-state electrolytes have enhanced the overall stability and ionic conductivity [39]. As a result, the PCE of the current state-of-the-art DSSCs based on two newly developed co-sensitizers has reached up to ~15.2% [40]. This, in turn, has expanded the potential applications of DSSCs to include indoor energy harvesting [41]. Despite these advancements, challenges remain in achieving competitive efficiency and long-term stability, prompting ongoing research and innovation in this field.

One such pressing issue arises from setbacks in one of the key DSSC components, the photoanode, which suffers from shortcomings of TiO_2 as the traditional semiconducting layer material. For example, TiO_2 displays poor light absorption in the visible region [42,43], which impairs electron-hole pair generation. TiO_2 also exhibits poor electron transport [43,44], which causes ineffective exciton dissociation with high recombination. This ultimately shortens the electron lifetime, resulting in state-of-the-art DSSCs with low PCEs that are ~58% of their first-generation counterparts (commercially available crystalline silicon solar cells) [45]. Additional major challenges are linked to Pt, the conventional counter electrode material, which is expensive due to its scarcity, and has poor stability in the electrolyte medium due to its low resistance to corrosion from I_3^- [46–50]. This increases the cost of DSSCs and shortens their lifetime.

Being motivated by this, significant research efforts have been recently directed towards developing potential alternatives to the traditional TiO_2 and Pt electrode materials, including semiconducting metal oxides [51,52], metal chalcogenides [53,54] and perovskites [55,56], with competitive photovoltaic performance, excellent stability and low-costs. However, on their own, these materials exhibit relatively low electrical conductivity [57,58], which lowers device performance. This, in turn, necessitates the integration of these alternative materials with highly conductive materials to facilitate synergistic interactions that help in overcoming the limitations of individual materials, while also complementing their merits to improve device performance.

One such promising class of conductive materials is the emerging carbon nanomaterials family [59–62], specifically graphene and its derivatives, including graphene oxide (GO) and reduced GO (rGO), which show facile synthesis procedures and remarkable physicochemical properties [63–67]. This benefits from the merits of graphene, including its high specific surface area, wide visible light absorption spectrum and high electrical conductivity [68,69]. These merits promote effective dye adsorption, enhanced photon harvesting and efficient electron transport with minimum recombination in DSSC photoanodes. Furthermore, the low charge transfer resistance and high electrocatalytic activity of graphene-based counter electrode nanomaterials are beneficial for enhancing the transfer of electrons from an external circuit to the electrolyte for catalyzing I_3^- reduction [70,71]. Most importantly, the high mechanical, thermal and chemical stabilities of graphene-based materials prolong the device lifespan [72,73]. On the other hand, their inexpensive nature owing to the inherent abundance of carbon lowers the device cost, and their non-toxicity allows for the fabrication of devices that are safe to use.

However, despite the promising potential of graphene-based composites with metal oxides, metal chalcogenides and perovskites to address the issues of traditional electrode materials in DSSCs, to the best of our knowledge, their practical application has been relatively less explored. Hence, this review seeks to advance the fabrication of efficient, durable and low-cost DSSCs by highlighting the recent breakthroughs in TiO_2-free photoanodes and Pt-free counter electrodes achieved during the last five-years (2020–2024), by employing the aforementioned graphene-based composite materials as photoanodes and counter electrodes. Merits, disadvantages and future research directions for developing TiO_2-free photoanodes and Pt-free counter electrodes are also discussed to provide a link-bridge for practical applications.

2. Graphene-based materials

Graphene, a two-dimensional semiconducting material, is made up of a single layer of sp^2-hybridized carbon atoms with a hexagonal lattice structure (Fig. 1(a)). Graphene has been commonly prepared using top-down approaches, e.g., exfoliation [74–81], where stacked graphite layers are separated into few layers of graphene sheets, and bottom-up approaches, e.g., chemical vapour deposition (CVD) [82–91], in which graphene is synthesized at high temperatures from either elemental carbon or carbon radicals. The application of graphene in photovoltaic devices has been made possible by its interesting properties, such as excellent stability, large specific surface area, tunable zero band gap, broad and intense absorption spectrum, high visible region transparency, and high electrical conductivity [92–98]. However, like other carbon-based materials, such as carbon nanotubes, nanospheres, nano-onions and nanofibers, graphene has limitations emanating from its hydrophobicity, insolubility and poor dispersion in many organic solvents due to its chemical inertness [99–101]. This makes graphene incompatible with low-cost solution processing during DSSC device fabrication. To overcome these drawbacks, the oxidation-reduction method has been recently used to prepare oxygen-functionalized derivatives of graphene, i.e., GO and rGO (Fig. 1(b-c)), with better solubility and dispersion than graphene.

The abundance of oxygen functional groups enhances the chemical reactivity of GO and renders GO with superior hydrophilicity and good dispersibility in many solvents, especially polar solvents, facilitating the compatibility of GO to low-cost solution processing [101,102]. Nonetheless, the oxygen-containing functional groups disrupt the conductive properties of GO, making it an insulator [103], which limits its application in DSSCs. Hence, GO is commonly reduced by removing some of its oxygen functional groups to prepare rGO. This restores electron delocalization and increases electrical conductivity. The remaining oxygen functional groups in rGO play a critical role in facilitating strong synergistic interactions with other active materials [104,105]. This not only enhances the stability of the resulting composite material, but also improves its optoelectronic properties. However, during reduction, electron delocalization is partially restored, which compromises the optoelectronic properties of rGO. Therefore, to optimize the optoelectronic properties of rGO and make them competitive to those of graphene in DSSC applications, rGO has been recently doped with heteroatoms, such as B and N [106], as well as being incorporated into novel semiconducting materials, including metal oxides [107], metal

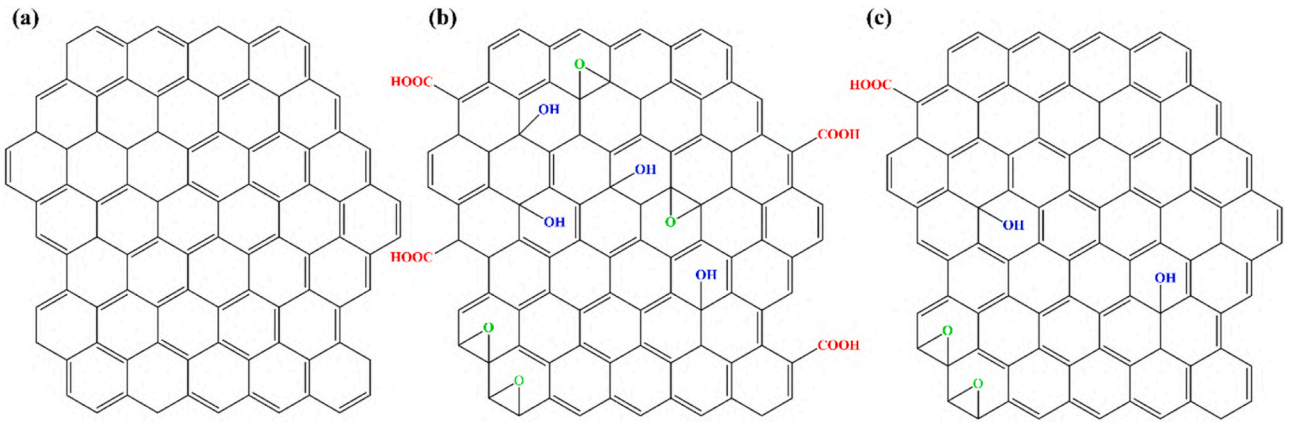

Fig. 1. Molecular structure of (a) graphene, (b) GO and (c) rGO.

chalcogenides [108] and perovskites [55], to form nanocomposites, as discussed in the following sections.

3. Photoanode

A dye-loaded semiconducting metal oxide material is deposited on a transparent conducting oxide material to prepare a DSSC photoanode responsible for photon-to-electricity conversion [109,110]. Thus, an efficient photoanode material should be highly transparent to allow for the entrance of more light into the cell. It must also be mesoporous with a high specific surface area to provide numerous active sites that effectively adsorb dye molecules for efficient light harvesting. A highly conductive photoanode also promotes rapid electron transport with minimum recombination. A photoanode material should also be constituted by relatively large particles to prevent unabsorbed light from being transmitted through the photoanode by scattering it back to the dye-coated semiconductor to facilitate effective photon harvesting. Furthermore, the photoanode should provide proper alignment of the conduction band with the lowest unoccupied molecular orbital (LUMO), i.e., it should be well below the dye LUMO to facilitate efficient electron transfer [111,112]. A good photoanode should also exhibit high stability in the electrolyte system to prolong the device lifetime.

An assortment of wide band gap semiconducting metal oxides, such as TiO_2 [113,114], Nb_2O_5 [115,116], SnO_2 [117,118] and ZnO [119,120], have been employed over the years to fabricate DSSC photoanodes. Among them, TiO_2 has been widely recognized as the conventional semiconducting layer material owing to its ease of availability and non-toxicity, which make it inexpensive [121–124], as well as its excellent photochemical stability [125–127], which increases device lifetime. Additionally, the mesoporous nature of TiO_2 provides the photoanode with a large surface area beneficial for enhancing dye adsorption.

Nevertheless, TiO_2 exhibits a relatively low optical transmittance in the visible region, which limits the passage of more light into the cell. TiO_2 also has a wide band gap (~3.2 eV), which permits the harvesting of ultraviolet (UV) light only, resulting in poor visible light absorption [128–130]. The TiO_2 wide band gap also provides a large energy barrier at the dye/semiconductor interface. This causes poor injection of electrons from the dye molecule LUMO to the TiO_2 conduction band, as well as high recombination of photogenerated electrons with oxidized dye molecules and I_3^- in the electrolyte. Thus, TiO_2 has been commonly integrated with highly transparent materials to increase its transmittance in the visible region, and medium or narrow band gap materials to reduce its band gap to extend the absorption spectrum from the UV to the visible region [131]. This enhances photon harvesting and promotes exciton generation. Medium or narrow band gap materials also lower the energy barrier at the dye/TiO_2 interface, which promotes the effective dissociation of electron-hole pairs and the efficient injection of photogenerated electrons from the LUMO of dye molecules to the TiO_2 conduction band with minimum recombination.

The small-sized TiO_2 nanoparticles show many defects and grain boundaries. These allow for the transmission of unabsorbed light through the photoanode due to their inability to effectively scatter unabsorbed light back to the photoanode, thereby causing poor photon harvesting. The numerous defects and grain boundaries also cause TiO_2 to have poor electron transfer properties with high recombination rates [132]. As a consequence, a light-scattering layer has been commonly prepared by introducing larger TiO_2 particles with dimensions comparable to the wavelength of visible light [133]. This prevents unabsorbed light from passing through the photoanode by reflecting it to the photoanode itself to enhance light harvesting for effective exciton generation to occur. TiO_2 has also been integrated with highly conductive materials, which provide additional electron transport pathways beneficial for improving electron transfer with low recombination losses [134]. In addition, post-synthesis treatments of TiO_2, e.g., with $TiCl_4$ solution [135], and thermal annealing [136], have also been employed to repair the surface defects, which, in turn, reduces the number of charge carrier scattering centres, resulting in rapid electron transport with minimum recombination.

The mesoporous TiO_2 film also permits direct contact between the electrolyte and bare sites of the transparent conducting electrode, resulting in recombination between I_3^- in the electrolyte and photogenerated electrons on the transparent conducting electrode [137]. This shortens the electron lifetime, leading to poor photovoltaic performance. As a result, a compact layer has been commonly deposited at the transparent conducting electrode/mesoporous TiO_2 interface to prevent direct contact between the electrolyte and the transparent conducting electrode to suppress recombination [138]. A compact layer also assists by smoothing out the transparent conducting electrode/TiO_2 interface, which reduces issues with short-circuits and leakage current; hence, increasing device performance.

Despite the aforementioned efforts to modify the photovoltaic performance of TiO_2, the PCE of state-of-the-art TiO_2-based DSSCs (~15.2%) [40] remains lower than that of commercialized first-generation (crystalline silicon) solar cells (>26%) [45]. As a result, recent research interests have shifted from TiO_2 to concentrate on emerging low-cost TiO_2-free semiconducting layer materials, such as metal oxides [139–141], metal chalcogenides [142,143] and perovskites [144–146], with competitive photovoltaic performance and stability. However, in their pristine form, these alternative materials tend to aggregate, resulting in small surface areas with poor dye adsorption, ineffective light harvesting and low electrical conductivity. These semiconducting materials also have drawbacks due to their wide band gap. On the one hand, wide band gap causes poor visible light absorption by permitting the absorption of UV light only. On the other hand, wide band gap provides a large energy barrier that inhibits the effective

injection of photogenerated electrons from dye molecules to the semiconducting material. This, in addition to the low charge transfer rate of these semiconducting materials, causes poor exciton dissociation and high recombination of electrons with I_3^- in the electrolyte and oxidized dye molecules, which shortens the electron lifespan, resulting in poor device performance.

Inspired by this, these semiconducting materials have recently been coupled with highly conductive carbon nanomaterials, particularly rGO, with a large specific surface area [147] to supply more active sites for effective dye loading to improve visible light absorption and electron-hole pair generation. This also takes advantage of the residual oxygen functionalized groups in rGO, which enable it to strongly bind with active materials to enhance charge transfer and device stability [104,105]. The introduction of rGO, a narrow band gap material, also helps to lower the band gap of the semiconducting material. This, in turn, widens the absorption spectrum to the visible region to improve light harvesting and electron-hole pair generation. Simultaneously, the energy barrier is lowered to enhance exciton dissociation and electron transfer with low recombination losses.

Similar to the above-mentioned pristine semiconducting materials, pristine rGO nanosheets tend to aggregate and restack [97,148], which reduces the photoanode surface area, resulting in poor dye loading and low photon absorption. This also compromises electron transport, giving rise to high recombination rates, and hence low short-circuit current density (J_{sc}) and PCE. Interestingly, the preparation of rGO-based composites with the aforementioned semiconductor materials helps to prevent the aggregation of the individual constituents. Therefore, it minimizes the loss of specific surface area, enhances dye loading and visible light absorption, and reduces interfacial charge transfer resistance. This not only helps to overcome the setbacks of the individual constituents, but also those of TiO_2, the traditional photoanode, as discussed in Section 4.

4. Reduced graphene oxide-based TiO_2-free photoanodes

The recent applications of rGO-based composites with semiconducting metal oxides, metal chalcogenides and perovskites, as promising alternatives to TiO_2 photoanodes in DSSCs, have been discussed in Sections 4.1–4.3 and summarized in Tables 1–3, respectively.

4.1. Reduced graphene oxide/metal oxide nanocomposites

Recently, rGO has been introduced into metal oxides, such as CuO, CdO, SnO_2, CeO_2 [149], Bi_2O_3 [150], ZnO [149,151–153], ZnO-Fe_2O_3 nanocomposites [154] and Sr-doped ZnO (Sr-ZnO) [155]. Among other advantages, the rGO sheets provide better energy band alignment at the dye/photoanode interface, which facilitates the fast transfer of photogenerated electrons from the LUMO of dye molecules to the metal oxide conduction band with minimum recombination. This increases the electrical conductivity of the photoanode, e.g., as demonstrated by the significant increase in the slope of the current-voltage (*I-V*) curves of rGO-based composites (Fig. 2(a)), which ultimately increases the J_{sc} (Fig. 2(b)), and hence improves the DSSC performance [150]. For example, DSSCs based on rGO/metal oxide composite photoanodes have recently displayed comparable photovoltaic performance to their traditional TiO_2-based counterparts, e.g., by reaching up to ~87% of the PCE of TiO_2 reference devices [149]. Also, the rGO/metal oxide-based DSSCs have surpassed the PCE of pristine metal oxide devices, e.g., by ~564% [150] and ~133% [153], demonstrating the significant role played by rGO towards improving device performance. Thus, rGO/metal oxide composites can be used in future research as promising alternatives to not only the conventional TiO_2 photoanodes, but also to their pristine metal oxide counterparts.

4.2. Reduced graphene oxide/metal chalcogenide nanocomposites

Metal chalcogenides, such as CuS [156], MoS_2 [157] and WS_2 [158], have also been integrated with rGO, and used as potential alternatives to the traditional TiO_2 photoanodes in DSSCs. Among other merits, the mesoporous nature of the resulting materials, revealed by the type IV N_2 adsorption-desorption isotherms with a characteristic H3 hysteresis loop (Fig. 3(a)) [157], provides a large photoanode surface area, which allows for optimum distribution of dye molecules on the semiconducting layer with minimum agglomeration. This, in addition to the large specific surface area of rGO, improves dye loading and increases visible light absorption for effective photogeneration of electrons to occur. At the same time, a significant reduction in pore diameter upon the formation of the composites was revealed by the Barrett-Joyner-Halenda (BJH) pore size distribution curves (Fig. 3(b)) [157]. This helps to

Table 1
Photovoltaic parameters of DSSCs using metal oxide and rGO/metal oxide nanocomposite photoanodes. V_{oc} and FF represent the open-circuit voltage and the fill factor of the solar devices, respectively.

Semiconducting layer material	Dye	Redox couple	V_{oc} (V)	J_{sc} (mA cm^{-2})	FF	PCE (%)	Ref.
CuO	N719	I^-/I_3^-	0.71	3.63	0.67	1.76	[149]
rGO/CuO			0.72	4.62	0.78	2.65	
CdO	N719	I^-/I_3^-	0.72	4.86	0.72	2.64	[149]
rGO/CdO			0.74	6.48	0.68	3.53	
SnO_2	N719	I^-/I_3^-	0.61	6.62	0.47	1.90	[149]
rGO/SnO_2			0.53	12.20	0.46	3.01	
CeO_2	N719	I^-/I_3^-	0.50	6.90	0.50	1.74	[149]
rGO/CeO_2			0.52	8.60	0.45	2.15	
Bi_2O_3	Eosin B	I^-/I_3^-	0.53	6.00	0.21	0.42	[150]
rGO/Bi_2O_3			0.48	9.80	0.44	1.68	
B-rGO/Bi_2O_3			0.59	10.00	0.50	2.79	
N-rGO/Bi_2O_3			0.55	9.20	0.47	1.97	
ZnO	N719	I^-/I_3^-	0.74	6.77	0.69	3.50	[149]
rGO/ZnO			0.73	8.52	0.70	4.44	
ZnO	N719	I^-/I_3^-	0.43	0.20	0.38	0.33	[151]
rGO/ZnO			0.46	0.24	0.52	0.57	
ZnO	N719	I^-/I_3^-	0.58	1.18	0.66	0.45	[152]
rGO/ZnO			0.54	1.60	0.56	0.50	
ZnO	N719	I^-/I_3^-	0.35	2.33	0.56	0.46	[153]
rGO/ZnO			0.39	4.65	0.59	1.07	
rGO/ZnO	N719	I^-/I_3^-	0.20	2.68	0.29	0.16	[154]
rGO/ZnO-Fe_2O_3			0.60	1.75	0.40	0.42	
ZnO	N719	I^-/I_3^-	0.58	6.40	0.51	1.90	[155]
rGO/ZnO			0.73	8.15	0.60	3.58	
rGO/Sr-ZnO			0.70	18.40	0.61	7.90	

Table 2
Photovoltaic parameters of DSSCs using metal chalcogenide and rGO/metal chalcogenide nanocomposite photoanodes.

Semiconducting layer material	Dye	Redox couple	V_{oc} (V)	J_{sc} (mA cm^{-2})	FF	PCE (%)	Ref.
CuS			0.64	11.10	0.56	4.27	
rGO	N719	I^-/I_3^-	0.48	9.20	0.48	2.08	[156]
rGO/CuS			0.71	16.00	0.70	7.81	
MoS_2			0.67	9.32	0.52	3.36	
rGO	N719	I^-/I_3^-	0.58	6.94	0.46	1.23	[157]
rGO/MoS_2			0.82	15.82	0.71	8.92	
WS_2			0.68	11.80	0.62	4.20	
rGO	N719	I^-/I_3^-	0.59	9.20	0.52	2.10	[158]
rGO/WS_2			0.79	18.60	0.66	9.60	

Table 3
Photovoltaic parameters of DSSCs using perovskite and rGO/perovskite nanocomposite photoanodes.

Semiconducting layer material	Dye	Redox couple	V_{oc} (V)	J_{sc} (mA cm^{-2})	FF	PCE (%)	Ref.
$ZnTiO_3$	N719	I^-/I_3^-	0.66	1.90	0.34	0.43	[159]
rGO/$ZnTiO_3$			0.65	4.27	0.40	1.11	
$SrTiO_3$	N719	I^-/I_3^-	0.76	6.98	0.49	2.59	[160]
rGO/$SrTiO_3$			0.77	11.16	0.63	5.42	
$BaTiO_3$	N719	I^-/I_3^-	0.73	7.50	0.56	3.07	[161]
rGO/$BaTiO_3$			0.73	15.02	0.54	5.92	
$BaSnO_3$	N719	I^-/I_3^-	0.67	11.01	0.52	3.82	[162]
rGO/$BaSnO_3$			0.70	13.96	0.57	5.59	
rGO	Eosin B	I^-/I_3^-	0.62	8.17	0.51	3.98	[163]
rGO/SSFC			0.74	13.15	0.59	7.01	

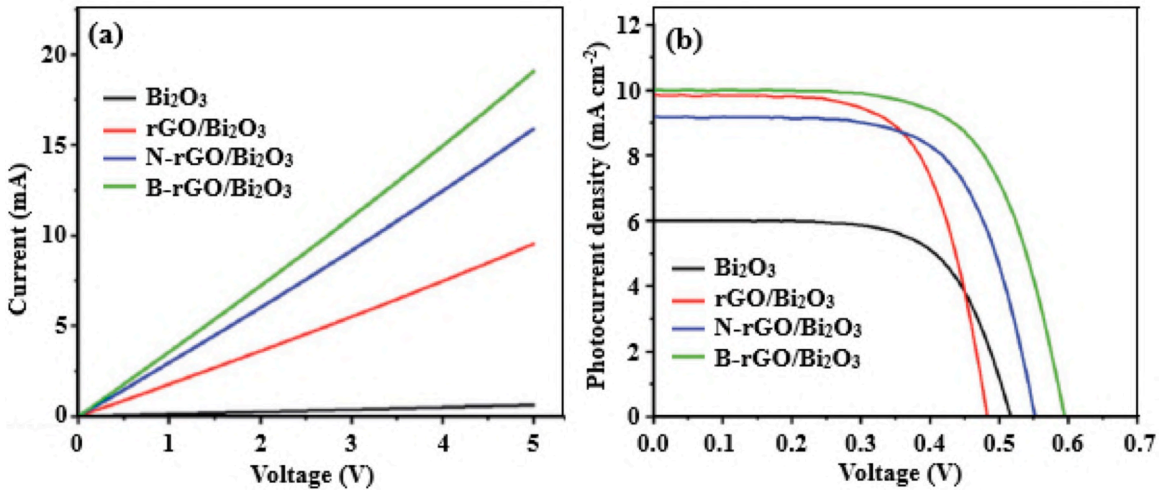

Fig. 2. (a) Current-voltage characteristics, and (b) photocurrent density-voltage curves of pristine Bi_2O_3 and rGO/Bi_2O_3-based composites. Adapted under a Creative Commons license [150], Copyright (2022), open access.

suppress the recombination of electrons on the transparent electrode and I_3^- in the electrolyte by reducing the amount of electrolyte that penetrates through the photoanode to reach the transparent electrode. Low charge carrier recombination favourably results in high electron density, which increases the J_{sc}, and causes a shift in the Fermi level, which increases the open-circuit voltage (V_{oc}), thereby increasing the PCE. For example, the rGO/WS_2 composite photoanode-based DSSCs displayed an optimum PCE of ~10%, which surpassed that of pristine WS_2- and rGO-based devices by ~129 and 357%, respectively [158], highlighting the superiority of rGO/metal chalcogenide composites.

The excellent chemical, mechanical and thermal stability of rGO is also beneficial for complementing the high stability of metal chalcogenides. This helps to increase the device lifetime, e.g., as demonstrated by the ability of rGO/CuS-based DSSCs to retain ~95% of the initial PCE after exposure to light illumination for 21 days [156]. This outperformed the devices based on pristine rGO and CuS photoanodes, which maintained ~85 and 88% of their original PCEs, respectively, under the same conditions. In a similar study, rGO/MoS_2-based DSSCs managed to maintain above 95% of the original PCE after a relatively longer period of 60 days (Fig. 4) [157]. Thus, the introduction of rGO into metal chalcogenides to form rGO/metal chalcogenide composites not only increases the device efficiency, but also enhances the device stability, both of which are critical for practical and commercial applications.

4.3. Reduced graphene oxide/perovskite nanocomposites

Perovskite metal oxide semiconductor materials, such as $ZnTiO_3$ [159], $SrTiO_3$ [160], $BaTiO_3$ [161], $BaSnO_3$ [162] and $Sr_{0.7}Sm_{0.3}Fe_{0.6}Co_{0.4}O_3$ (SSFC) [163], have also been recently employed in combination with rGO, as promising alternatives for TiO_2 photoanodes in DSSCs. In addition to other advantages, this helps to prevent the aggregation of pristine perovskite oxide nanoparticles (Fig. 5(a)) and the restacking of wrinkled rGO sheets (Fig. 5(b)) [163], which would otherwise reduce

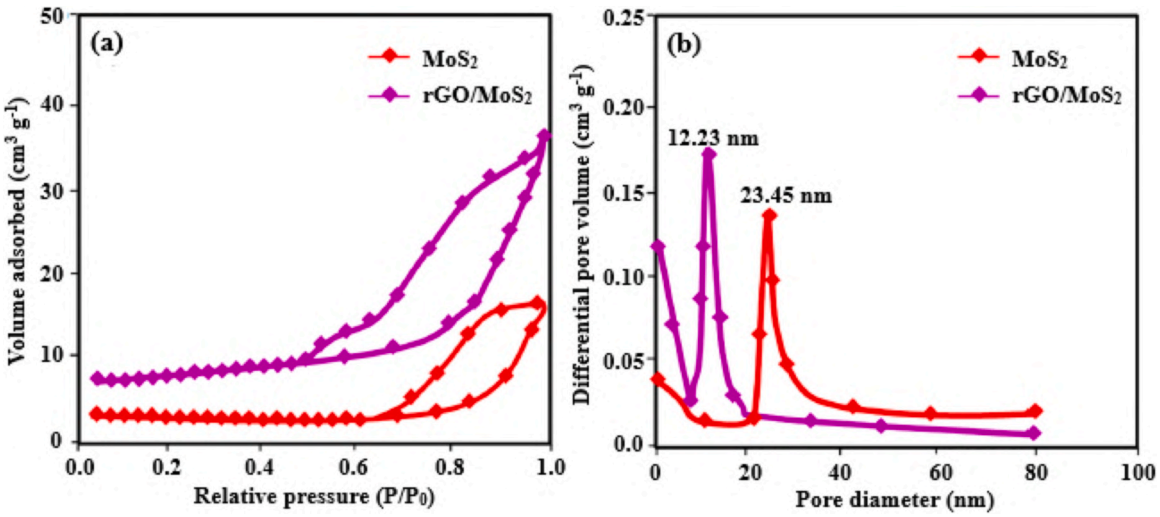

Fig. 3. (a) N_2 adsorption-desorption analysis, and (b) pore size distribution of pristine MoS_2 and the rGO/MoS_2 composite. Adapted from [157], Copyright (2020), with permission from Elsevier.

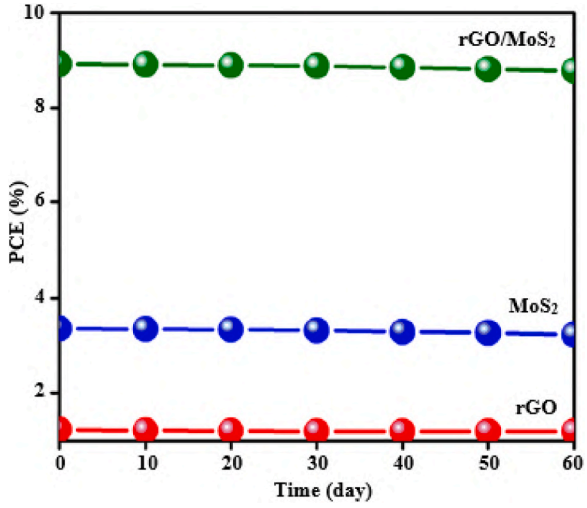

Fig. 4. Stability test of rGO-, MoS_2- and rGO/MoS_2-based DSSCs. Adapted from [157], Copyright (2020), with permission from Elsevier.

the specific surface area of the photoanode, compromise dye loading and impede electron transport. As a result, the prepared nanocomposites were made up of a homogeneous dispersion of perovskite oxide nanoparticles on the rGO nanosheets (Fig. 5(c)) [163], which allowed for the provision of numerous active sites for not only improving the adsorption of dye molecules, but also for enhancing electron transport on the rGO/perovskite oxide nanocomposite surface.

When compared to pristine perovskite oxides, the superior dye-loading capacity of rGO/perovskite oxide composites is demonstrated in Fig. 6(a) by the higher absorbance of N719 dye molecules desorbed from the surface of rGO/$BaTiO_3$ composites [161]. This indicates that the rGO/$BaTiO_3$ composites initially adsorb more dye than pristine $BaTiO_3$ before desorption. Effective dye loading enhances light harvesting, which, in turn, improves exciton generation. This, in addition to the conductive nature of rGO, ensures effective exciton dissociation with minimum recombination, as revealed by the decrease in photoluminescence (PL) intensity (Fig. 6(b)) [161], thereby improving device performance. For example, DSSCs based on rGO/perovskite oxide composite photoanodes have managed to exceed the PCE of the pristine rGO, e.g., by ~71% [163], and pristine perovskite oxides, e.g., by ~109% [160]. Therefore, rGO has significant potential to improve the performance of perovskite oxide photoanode materials in DSSCs.

5. Counter electrode

A conductive and catalytic material is deposited on a transparent conducting oxide material to prepare a DSSC counter electrode responsible for transferring electrons from an external circuit to the electrolyte to speed up the reduction of I_3^- to I^- for the subsequent regeneration of dye molecules [164–167]. Thus, a good counter electrode material should be highly conductive to enable the rapid transfer of electrons to the electrolyte, and highly electrocatalytic to speed up I_3^- reduction. An efficient counter electrode should also be highly reflective to prevent the loss of unabsorbed light transmitted through the photoanode by reflecting it to the sensitizer (dye molecules) to promote effective photon harvesting. Additionally, the counter electrode should be highly stable in the electrolyte system to prolong the device lifespan.

Meanwhile, Pt thin films deposited on a transparent conducting electrode have been widely used as the conventional counter electrode due to their high reflectance, low charge transfer resistance, high electrical conductivity and high electrocatalytic activity [168–171]. Nonetheless, Pt suffers from high-costs owing to its scarcity, and instability issues due to its poor corrosion resistance to I_3^- in the redox couple [172–181]. Although considerable research efforts have been made to improve device performance and stability, using approaches which include fabricating Pt-based nanocomposites with competitive electrical conductivity and electrocatalytic activity [182–184], the PCE and stability of Pt-based DSSCs have remained low. Therefore, the development of highly stable and low-cost Pt-free counter electrode materials with comparable electrical conductivity and electrocatalytic activity has recently emerged as one of the most promising strategies to overcome the aforementioned limitations.

Being motivated by this, numerous promising Pt-free counter electrode materials, such as metal oxides [185–187], metal chalcogenides [188–190] and perovskites [172,191], have been recently explored. This is primarily owing to their ability to facilitate electron hopping transport, which renders them with good electrocatalytic activity towards I_3^- reduction, in addition to their low-costs and excellent stability [192]. These alternative materials also have hierarchical structures with nanopores that allow for the exposure of more surface-active sites for electrocatalytic reactions, which speeds up the reduction of I_3^-. However, when compared to the conventional Pt counter electrode, the semiconducting nature of these alternative materials makes them have relatively low electrical conductivity and catalytic reduction

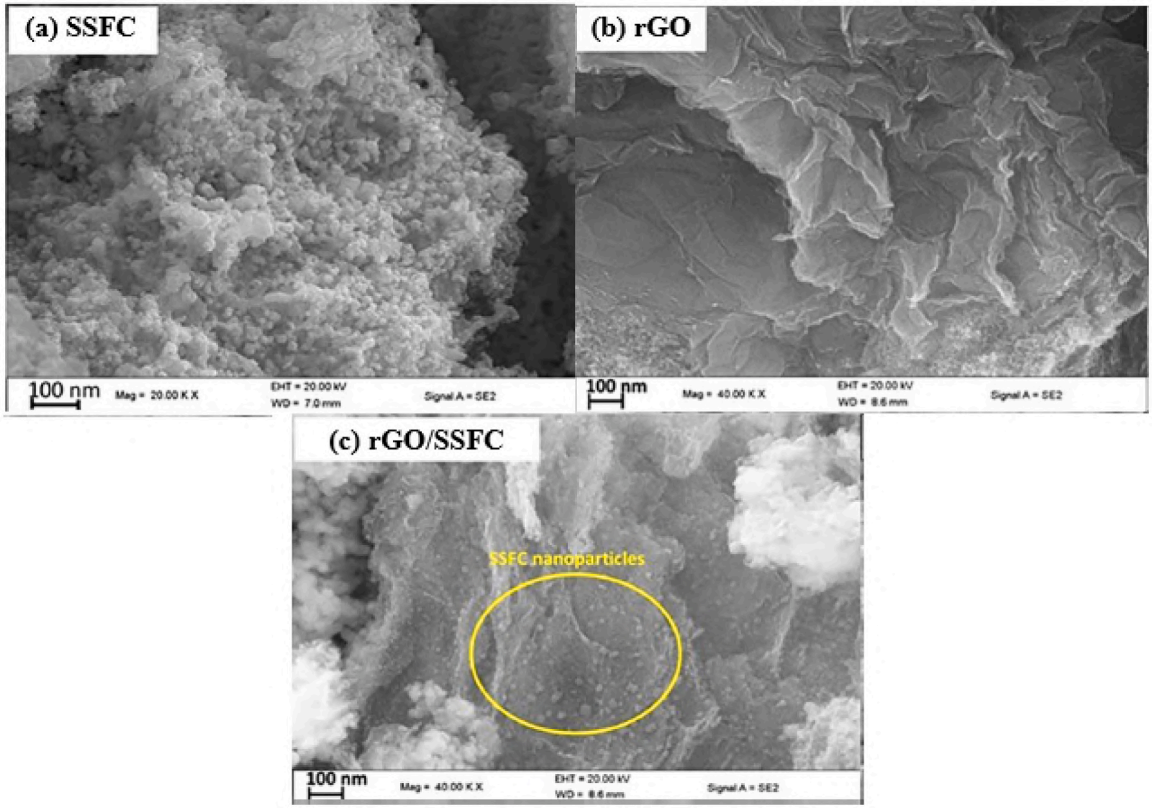

Fig. 5. Field-emission scanning electron micrographs of (a) SSFC, (b) rGO, and (c) rGO/SSFC. Adapted under a Creative Commons license [163], Copyright (2023), open access.

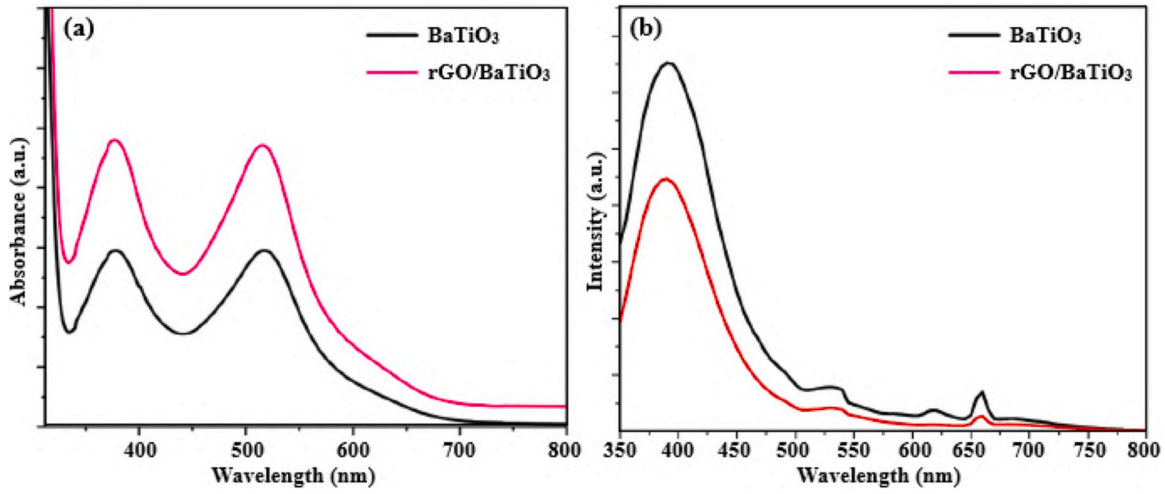

Fig. 6. (a) Absorption spectra of N719 dye molecules desorbed from the surface of pristine $BaTiO_3$ and rGO/$BaTiO_3$ composites, and (b) PL spectra of corresponding materials. Adapted from [161], Copyright (2024), with permission from Elsevier.

performance [174], both of which impair device performance. Thus, these alternative catalytic materials have been recently integrated with highly conductive and stable carbon nanomaterials, especially graphene-based materials, in particular, rGO, which is compatible with low-cost solution synthesis [193,194], to produce a significant enhancement in photovoltaic performance as discussed in Section 6.

6. Reduced graphene oxide-based Pt-free counter electrodes

The recent applications of rGO-based composites with semiconducting metal oxides, metal chalcogenides and perovskites, as potential replacements for Pt counter electrodes in DSSCs, have been discussed in Sections 6.1–6.3 and summarized in Tables 4–6, respectively.

6.1. Reduced graphene oxide/metal oxide nanocomposites

Recently, rGO has been introduced into various metal oxide-based counter electrodes, such as Co_3O_4 [195], Fe_3O_4 [192], α-Fe_2O_3 [196], MnO_2/NiO/CuO [197] and $Cu_2ZnNiSe_4/WO_3$ [198]. Among several advantages, this enables the large specific surface area and residual oxygen functionalized groups in rGO to support the uniform dispersion

Table 4
Photovoltaic parameters of DSSCs using metal oxide and rGO/metal oxide nanocomposite counter electrodes.

Counter electrode material	Dye	Redox couple	V_{oc} (V)	J_{sc} (mA cm^{-2})	FF	PCE (%)	Ref.
Co_3O_4			0.42	8.30	0.19	0.87	
rGO	N719	I^-/I_3^-	0.71	16.02	0.26	3.05	[195]
rGO/Co_3O_4			0.78	15.92	0.57	7.08	
rGO/Fe_3O_4	N719	I^-/I_3^-	0.72	5.18	0.59	2.20	[192]
α-Fe_2O_3			0.64	13.30	0.55	4.69	
rGO	N3	I^-/I_3^-	0.56	12.47	0.45	3.08	[196]
rGO/α-Fe_2O_3			0.65	15.43	0.61	6.12	
rGO/MnO_2/NiO/CuO	N719	I^-/I_3^-	0.75	13.46	0.76	7.67	[197]
rGO/$Cu_2ZnNiSe_4$/WO_3	N719	I^-/I_3^-	0.88	24.70	0.56	12.16	[198]

Table 5
Photovoltaic parameters of DSSCs using metal chalcogenide and rGO/metal chalcogenide nanocomposite counter electrodes.

Counter electrode material	Dye	Redox couple	V_{oc} (V)	J_{sc} (mA cm^{-2})	FF	PCE (%)	Ref.
$NiSe_2$	N719	I^-/I_3^-	0.62	12.20	0.50	6.04	[199]
rGO/$NiSe_2$			0.80	20.10	0.76	10.60	
$Ni_{0.85}Se$			0.74	15.88	0.66	7.76	
rGO	N719	I^-/I_3^-	0.71	6.88	0.59	2.88	[200]
rGO/$NiSe_2$			0.77	16.33	0.71	8.93	
$Cu_2ZnNiSe_4$	N719	I^-/I_3^-	0.68	17.50	0.33	3.88	[198]
rGO/$Cu_2ZnNiSe_4$			0.86	21.21	0.48	8.75	
rGO/Ni_2P_5	N719	I^-/I_3^-	0.70	16.94	0.60	7.02	[201]
rGO/$Ni_{12}P_5$			0.70	19.55	0.60	8.19	
rGO	N719	I^-/I_3^-	0.62	6.42	0.57	2.25	[202]
rGO/MoS_2			0.72	6.91	0.64	3.19	
MoS_2	N719	I^-/I_3^-	0.72	13.60	0.51	5.00	[203]
rGO			0.73	13.90	0.52	5.20	
rGO/MoS_2			0.71	14.20	0.62	6.30	
MoS_2	N719	I^-/I_3^-	0.73	4.52	0.61	2.01	[204]
rGO/MoS_2			0.74	7.80	0.68	3.92	
rGO/N-GQD/MoS_2			0.76	8.62	0.70	4.65	
rGO	N719	I^-/I_3^-	0.68	5.76	0.42	1.66	[205]
rGO/NiS_2			0.67	9.02	0.52	3.16	
$CoNi_2S_4$	N719	I^-/I_3^-	0.61	13.14	0.72	5.78	[206]
rGO			0.55	10.68	0.58	3.44	
rGO/$CoNi_2S_4$			0.67	16.34	0.84	9.22	
$CoNi_2S_4$	N719	I^-/I_3^-	0.62	8.41	0.66	3.45	[207]
rGO/$CoNi_2S_4$			0.88	21.96	0.85	10.21	
$FeNi_2S_4$	N719	I^-/I_3^-	0.60	8.01	0.63	4.87	[208]
rGO/$FeNi_2S_4$			0.87	20.04	0.84	9.98	

of metal oxide nanoparticles possibly through chemical bonds. This results in the even distribution of catalytic metal oxide nanoparticles on the surface of conductive rGO sheets. For instance, the integration of spherically-shaped and agglomerated α-Fe_2O_3 nanoparticles of diameter 20–50 nm (Fig. 7(a)) with wrinkled and folded rGO sheets (Fig. 7(b)) led to the formation of evenly decorated α-Fe_2O_3 nanoparticles on the surface of the rGO sheets (Fig. 7(c)) [196]. This demonstrates the presence of a strong interaction between rGO sheets and metal oxide nanoparticles, which is beneficial for the efficient collection and transfer of photogenerated electrons. Moreover, the resulting rGO/α-Fe_2O_3 composite film surface (Fig. 7(c)) exhibited a rough surface with numerous pores that are desirable for providing a large specific surface area with abundant oxidation sites for rapid I_3^- reduction. Therefore, in the rGO/metal oxide composite counter electrodes, the rGO sheets play a critical role by providing high-speed pathways for rapid electron transfer, while at the same time, the multilayer metal oxide

Table 6
Photovoltaic parameters of DSSCs using perovskite and rGO/perovskite nanocomposite counter electrodes.

Counter electrode material	Dye	Redox couple	V_{oc} (V)	J_{sc} (mA cm^{-2})	FF	PCE (%)	Ref.
rGO/La_2CrFeW_6/SO_4^{2-}	N719	I^-/I_3^-	0.65	22.00	0.53	7.59	[191]
rGO/La_2CrFeW_6/$CO(NH_2)_2$			0.67	22.40	0.56	8.40	
rGO/La_2CrFeW_6/CdSe			0.68	21.80	0.62	9.20	
rGO/La_2CrFeW_6/$C_6H_{10}S_3$			0.68	26.10	0.59	10.40	
SSFC	Eosin B	I^-/I_3^-	0.73	12.44	0.40	4.06	[209]
rGO			0.64	10.38	0.49	3.29	
rGO/SSFC			0.81	16.04	0.66	5.94	
N-rGO/SSFC			0.88	18.63	0.69	6.64	

nanoparticles on the rGO sheet surface provide numerous catalytically active sites for effective I_3^- reduction. Thus, the synergistic effects between the high electrocatalytic activity of metal oxides and the high electrical conductivity of rGO have the potential to improve the performance of Pt-free counter electrodes to compete with their Pt-based counterparts.

For example, DSSCs based on novel and low-cost rGO/metal oxide composite counter electrodes have recently exhibited comparable photovoltaic performance to those based on the traditional Pt counter electrode, e.g., reaching up to ~97% [195], ~93% [197], and ~88% [196] of the PCE of Pt-based reference devices. When compared to the rGO-based devices, the relatively high PCE of Pt reference devices can be ascribed to the superior electrical conductivity and electrocatalytic activity of Pt. The relatively low PCE of rGO-based devices can also be attributed to the poor reflectance of rGO-based counter electrodes. Poor reflectance prevents the reflection of unabsorbed incident light back to the photoanode. This contrasts with Pt, which has high reflectivity and facilitates the maximum utilization of unabsorbed incident light by reflecting it to the photoanode for electron-hole pair generation. Interestingly, the rGO/metal oxide-based devices outperformed their pristine metal oxide counterparts, e.g., by ~714% [195], and their pristine rGO-based DSSCs, e.g., by ~99% [196], demonstrating the critical role played by nanocompositing in improving device performance.

6.2. *Reduced graphene oxide/metal chalcogenide nanocomposites*

In recent years, rGO has been incorporated into metal chalcogenide counter electrodes, including selenides, e.g., $NiSe_2$ [199,200] and $Cu_2ZnNiSe_4$ [198]; phosphides, e.g., Ni_2P_5 and $Ni_{12}P_5$ [201]; sulfides, e.g., MoS_2 [202–204], NiS_2 [205], $CoNi_2S_4$ [206,207] and $FeNi_2S_4$ [208]. The successful formation of rGO/metal chalcogenide composites was confirmed by the appearance of characteristic diffraction peaks of both rGO and metal chalcogenides, e.g., NiS_2, in the XRD pattern of the composite (Fig. 8(a)) [205]. The presence of rGO in the composites was also confirmed by the appearance of *D*- and *G*-bands on the Raman spectra of the composites, e.g., rGO/NiS_2 (Fig. 8(b)). The *D*-band is associated with the presence of defects or disordered layers, while the *G*-band is ascribed to the presence of an ordered graphitic sp^2 carbon matrix. While the difference in the I_D/I_G ratio between the composite (1.07) and pristine rGO (1.04) may seem small and could fall within the error margin, it suggests the introduction of structural defects that enhance coupling between the conductive rGO sheets and catalytic metal chalcogenide nanoparticles, potentially providing more active sites for I_3^- reduction.

The rGO sheets also form highly conductive networks that connect

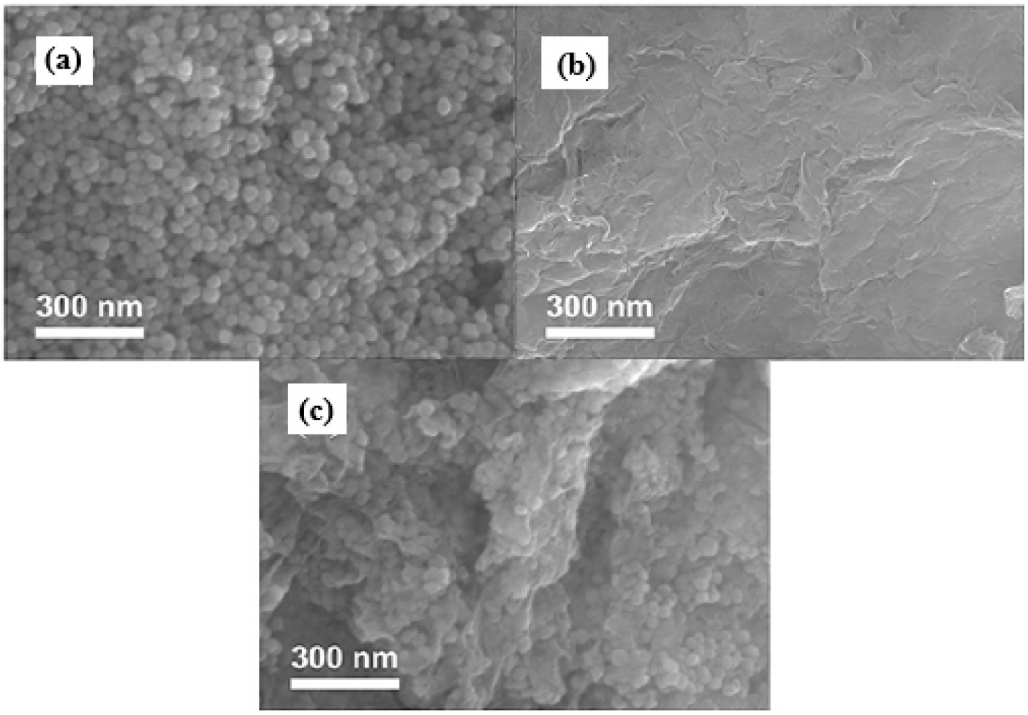

Fig. 7. Field-emission scanning electron micrographs of (a) α-Fe_2O_3, (b) rGO and (c) rGO/α-Fe_2O_3 composites. Adapted under a Creative Commons license [196], Copyright (2022), open access.

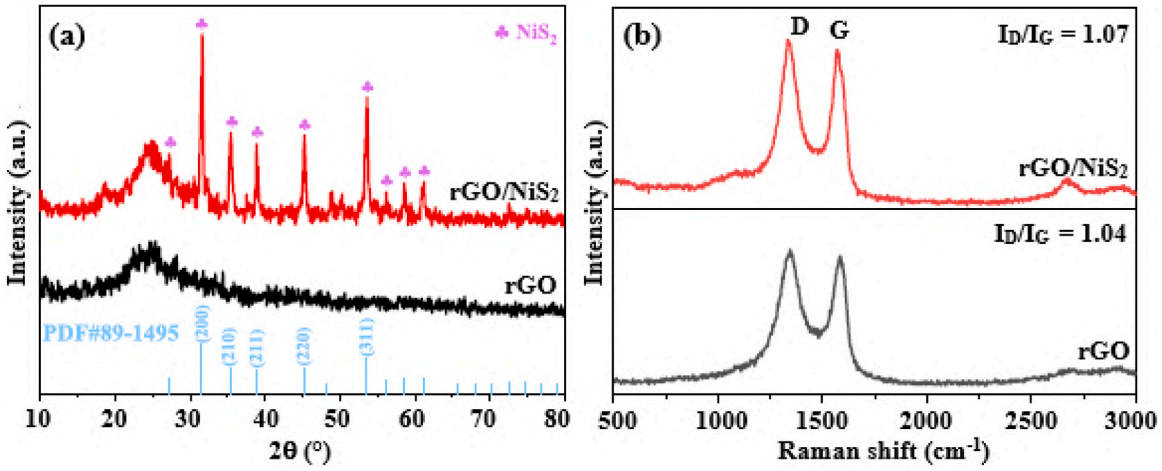

Fig. 8. (a) XRD diffractograms and (b) Raman spectra of pristine rGO and rGO/NiS_2 composites. Adapted from [205], Copyright (2023), with permission from Elsevier.

the metal chalcogenide nanoparticles and provide additional electron transport pathways. This reduces the charge transfer resistance (R_{ct}) at the counter electrode/electrolyte interface, e.g., as shown in the Nyquist plots from electrochemical impedance spectroscopy (EIS) analysis (Fig. 9(a)) [201], by the smaller diameter of the semicircle in the high-frequency region. This, in turn, facilitates the rapid transfer of electrons for catalyzing I_3^- reduction. Thus, when compared to Pt (0.83 Ω), the smaller R_{ct} (0.79 Ω) observed for the rGO/$Ni_{12}P_5$ composite indicates an increased electrocatalytic ability for I_3^- reduction due to the rapid charge-transfer process. Also, since the intercept of the semicircle in the high-frequency region with the real axis is numerically equal to the series resistance (R_s), largely affected by film adhesion to the substrate; the smaller R_s (11.56 Ω) of rGO/$Ni_{12}P_5$ than that of Pt (12.13 Ω) might have originated from the strong adhesion of the composite film to the substrate.

The electrocatalytic activity of the counter electrode materials for I_3^- reduction has been evaluated using cyclic voltammetry (CV), and compared with the Pt reference curve, consisting of two pairs of redox peaks. In Fig. 9(b) [201], the redox peaks at a relatively high potential correspond to the oxidation and reduction peaks of I_3^-/I_2, while those at a relatively low potential correspond to the oxidation and reduction peaks of I^-/I_3^-. Since electrons from the external circuit play a prominent role in reducing I_3^- to I^- during an electrochemical process, the redox peaks at a relatively low potential represent the electrocatalytic capabilities of the counter electrode. Also, since the magnitude of the peak current density (J_p) and peak-to-peak separation potential (ΔE_{pp}) are correlated to the capacity of the counter electrode to transfer electrons for reducing I_3^- species and the reversibility of the redox reaction, respectively, the higher J_p and smaller ΔE_{pp} observed for rGO/$Ni_{12}P_5$ indicate its faster reduction reaction kinetics and better electrochemical

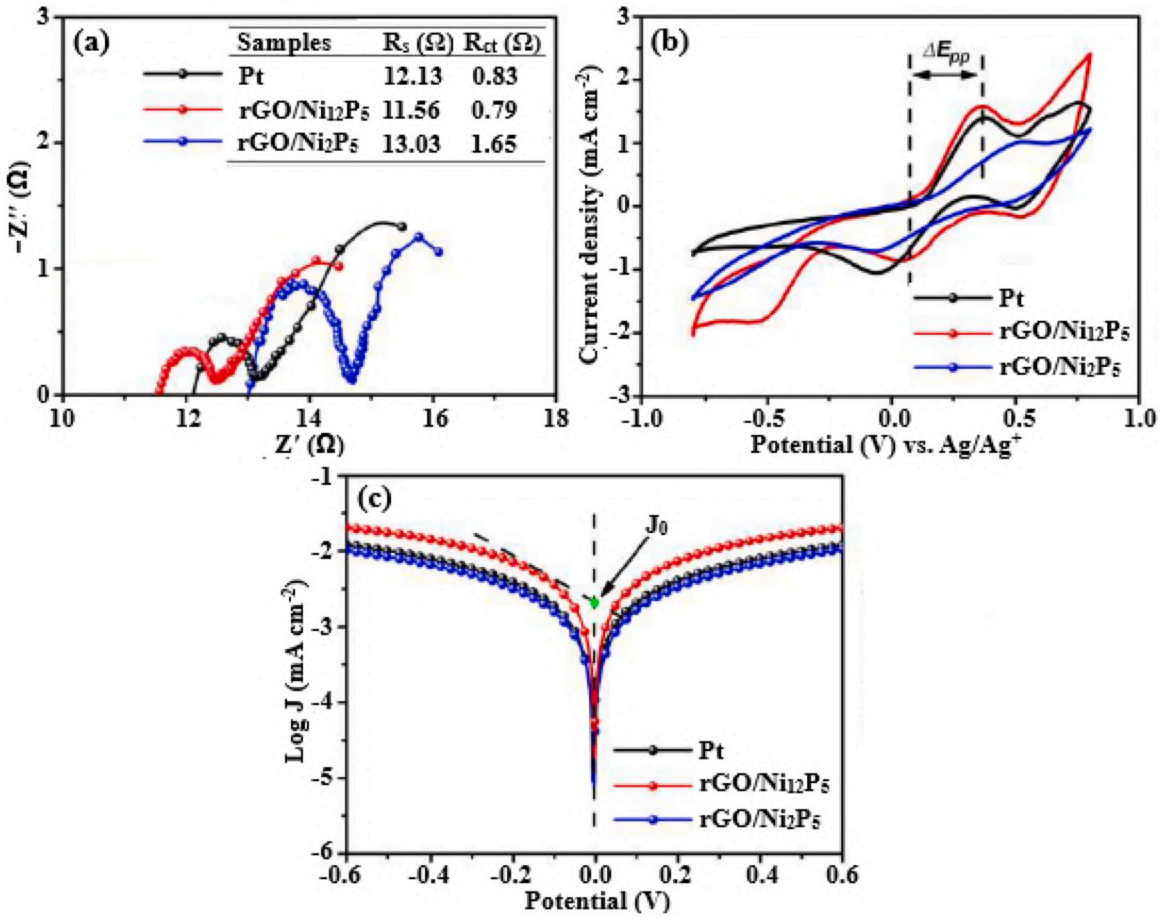

Fig. 9. (a) Nyquist plots, (b) cyclic voltammograms and (c) Tafel polarization curves of rGO/Ni_2P_5, rGO/$Ni_{12}P_5$ and Pt counter electrodes. Adapted from [201], Copyright (2020), with permission from American Chemical Society.

reversibility than those for Pt and rGO/Ni_2P_5. Therefore, the rGO/$Ni_{12}P_5$ composites exhibited outstanding electrocatalytic activity and faster response rates than those of Pt and rGO/Ni_2P_5. In addition, the appearance of a larger integral area on the CV curve of rGO/$Ni_{12}P_5$ composites compared to those of Pt and rGO/Ni_2P_5 demonstrates the potential of the rGO backbone to induce additional electrochemical processes, which ultimately enhance the electrochemical capacity of the $Ni_{12}P_5$ counter electrode. Thus, the competitive electrocatalytic activity of rGO/metal chalcogenide composites could make them effective alternatives to Pt counter electrodes in future research.

The electrocatalytic activity for I_3^- reduction has also been evaluated from the Tafel polarization curves by determining the exchange current density (J_0) in the Tafel region, from the intersection of the tangent of the cathodic branch and the equilibrium potential line (Fig. 9(c)), according to Eq. (1) [201]:

$$J_0 = \frac{RT}{nFR_{ct}} \quad (1)$$

where R is the universal gas constant, T is the absolute temperature, n is the number of electrons involved in the electrochemical reduction of I_3^-, F is Faraday's constant, and R_{ct} is the charge transfer resistance. J_0 is correlated to the rate of electron transfer between the electrode and the redox species, and it serves as an indicator of the electrocatalytic activity of a counter electrode. From Fig. 9(c), the steeper the slope of the cathodic branch in the Tafel zone, the greater the J_0 and the higher the catalytic activity of a material. Hence, the rGO/$Ni_{12}P_5$ composite exhibited the largest J_0 in the Tafel zone, followed by Pt and rGO/Ni_2P_5. This was consistent with EIS data, which showed a decrease in R_{ct} in the order from rGO/Ni_2P_5 (1.65 Ω), Pt (5.42 Ω) to rGO/$Ni_{12}P_5$ (0.83 Ω). A small R_{ct} is desirable since it enables a large number of electrons to be transferred through the counter electrode/electrolyte interface. Therefore, when compared to Pt and rGO/Ni_2P_5 counter electrodes, the rGO/$Ni_{12}P_5$ composite counter electrode (with smaller R_{ct} and larger J_0) displayed higher electrocatalytic activity, demonstrating the effectiveness of the composites in reducing I_3^-.

As a consequence, DSSCs based on the rGO/metal chalcogenide composite counter electrode have surpassed the PCE of Pt reference devices, e.g., by ~60% [207,208], and in some cases reached up to ~90% [202,203] and ~97% [206] of the PCE of Pt-based control devices. Moreover, the rGO/metal chalcogenide-based devices outperformed the pristine metal chalcogenide devices, e.g., by ~196% [207], and pristine rGO devices, e.g., by ~168% [206]. The enhanced device performance can be attributed to the ability of the composite counter electrode to exploit both the high electrical conductivity of rGO and the high electrocatalytic activity of metal chalcogenides.

The introduction of highly stable rGO sheets into metal chalcogenides also enhanced the long-term stability of DSSCs, e.g., as revealed by the ability of rGO/$NiSe_2$- [199], rGO/MoS_2- [202] and rGO/NiS_2-based devices [205] to maintain above 95% of the original PCE after storage for 60, 10 and 30 days, respectively. Additionally, no noticeable changes in J_p and ΔE_{pp} appeared in the CV curves of the composite after 10000 cycles at a scan rate of 10 mV s^{-1} (Fig. 10 (a)), while also the R_{ct} showed only a slight increase by ~7% (Fig. 10 (b)) [206], under the same conditions, demonstrating the robust electrochemical stability of the composite counter electrode. This was consistent with similar studies [27,108,200,202], which reported the fabrication of rGO/metal chalcogenide composite counter electrodes with superior electrochemical stability to their individual constituents. The excellent electrochemical

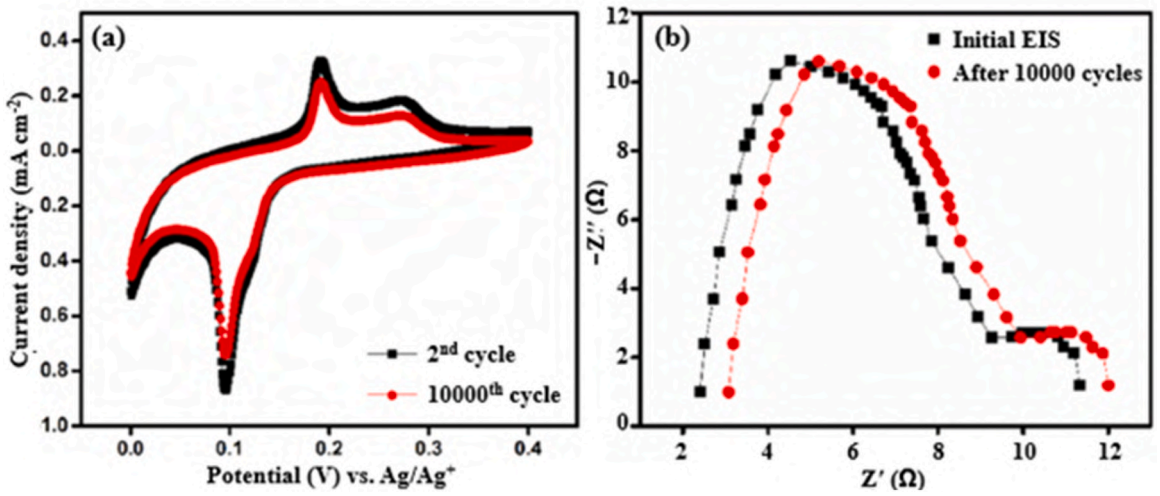

Fig. 10. (a) Cyclic voltammograms and (b) Nyquist plots of the rGO/$CoNi_2S_4$ composite (initial and after 10000 cycles). Adapted from [206], Copyright (2020), with permission from Elsevier.

stability of the composite electrode and long-term stability of the device are primarily owing to the presence of residual oxygen functionalized groups in rGO, which allows for the tight chemical anchoring of metal chalcogenide nanoparticles on the highly stable rGO sheet surface. This enables the rGO sheets to prevent the agglomeration and corrosion of counter electrode materials, while also the metal chalcogenide nanoparticles prevent the restacking of rGO sheets.

6.3. *Reduced graphene oxide/perovskite nanocomposites*

Perovskite materials, such as La_2CrFeW_6 [191] and SSFC [209], have been recently integrated with rGO, and used as counter electrode

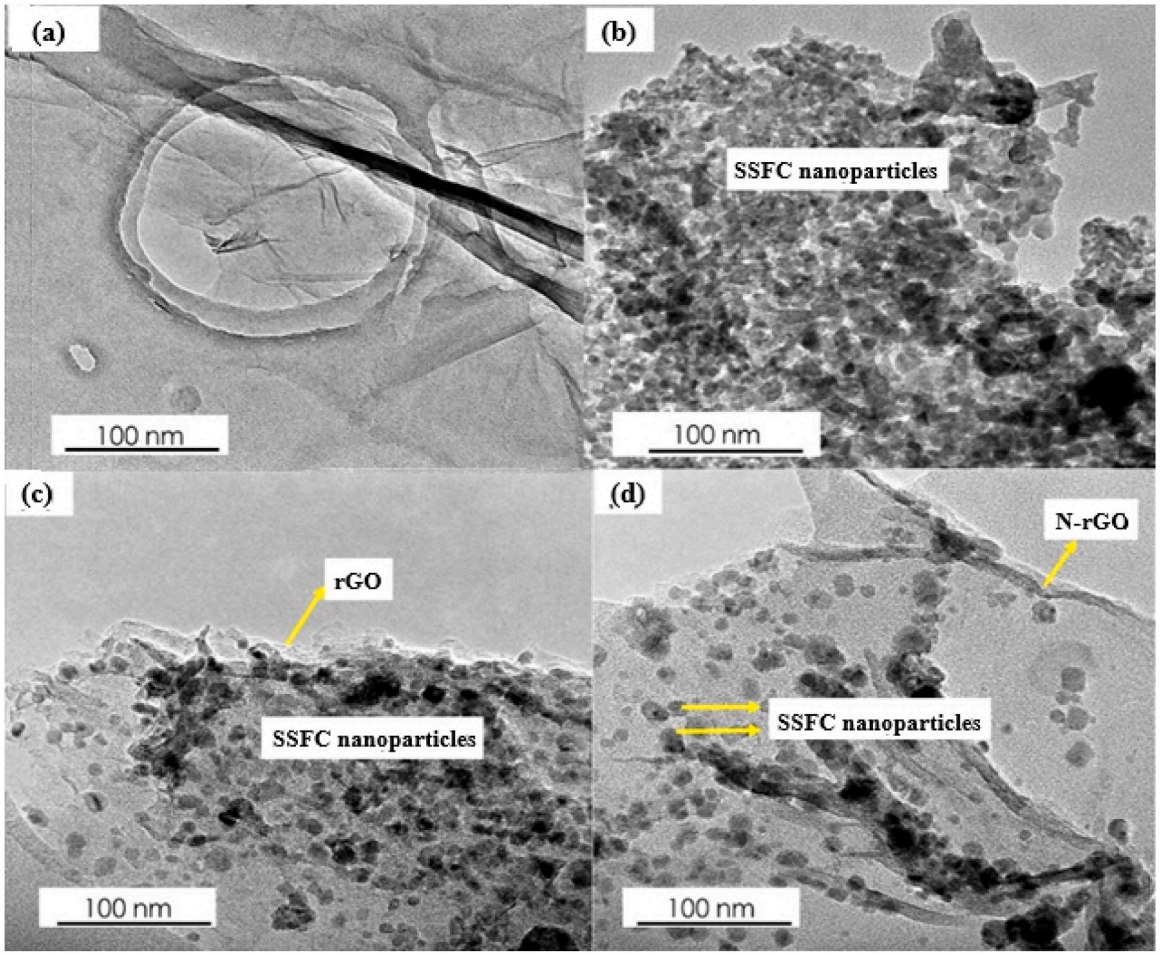

Fig. 11. Transmission electron microscopy images of (a) rGO, (b) SSFC, (c) rGO/SSFC and (d) N-rGO/SSFC. Adapted under a Creative Commons license [209], Copyright (2023), open access.

materials in Pt-free DSSCs. Among other merits, this enables the rGO sheets to help minimize perovskite nanoparticle aggregation, while at the same time, the perovskite nanoparticles help to prevent the restacking and aggregation of rGO sheets. For example, the recent introduction of wrinkled and folded rGO nanosheets (Fig. 11 (a)) into agglomerated SSFC perovskite nanoparticles of diameter ~24 nm (Fig. 11 (b)) led to the formation of well-dispersed and evenly decorated SSFC nanoparticles on the rGO (Fig. 11 (c)) and N-rGO nanosheet surfaces (Fig. 11 (d)) [209]. This ultimately renders the composite counter electrode with a larger surface area capable of enhancing the electroactive sites for the effective reduction of I_3^-.

Simultaneously, the rGO nanosheets provide the counter electrode with additional electron transport pathways, which lower the R_{ct}, and hence suppress recombination, as illustrated by the pronounced quenching of PL intensity in Fig. 12 [209]. It is interesting to note that recombination suppression through compositing was beneficial to both components and this suggests favourable chemical interactions between them. This enables the fast transfer of electrons from an external circuit to the electrolyte, which, in turn, catalyzes the reduction of I_3^-. The N-doped rGO composite is noteworthy for its relatively outstanding quenching performance of PL (Fig. 12 (b)). Consequently, this has led to the fabrication of rGO/perovskite composite-based devices with high PCEs, e.g., of ~7% [209] and ~10% [191], which not only outperformed the Pt-based reference device by ~20% [209] and 39% [191], but also the pristine SSFC and rGO devices by ~64 and 102%, respectively [209]. This demonstrates the potential of rGO/perovskite composites for use as Pt-free counter electrode materials in future DSSCs.

7. Conclusions and perspectives

When compared to commercially available crystalline silicon solar cells with a PCE of >26%, the commercial application of DSSCs continues to be hampered by their low PCE (~15.2%) mainly due to the shortcomings of traditional electrode materials, i.e., TiO_2 and Pt. Among other issues, TiO_2 has a relatively low visible region transparency, which restricts the passage of more light into the DSSC. In addition, the wide band gap of TiO_2 (~3.2 eV) permits only UV light absorption, and also provides a large energy barrier that causes poor electron transfer at the dye/semiconductor interface. This causes the recombination of photogenerated electrons with oxidized dye molecules and I_3^- in the electrolyte. The small-sized mesoporous TiO_2 nanoparticles also have numerous defects and grain boundaries, which cause ineffective scattering of unabsorbed light back to the photoanode, poor light absorption, and poor electron transfer with high recombination. To circumvent these drawbacks, TiO_2 has been used in combination with transparent and narrow or medium band gap materials to enhance visible region transparency, reduce the band gap and broaden the absorption spectrum to the visible region. This also helps to minimize the energy barrier at the dye/TiO_2 interface, thereby facilitating the effective dissociation of photogenerated charge carriers and the subsequent transfer of photogenerated electrons with low recombination. Additionally, light-scattering and compact layers have been developed to ensure the maximum utilization of absorbed light by scattering it back to the photoanode, while also preventing direct contact between the electrolyte and the transparent electrode to suppress recombination. The integration of TiO_2 with highly conductive nanomaterials to provide additional electron transport pathways, as well as the post-synthesis treatment of TiO_2 to repair surface defects and improve electron transport, have also been employed to address the setbacks of TiO_2. On the other hand, Pt, the traditional counter electrode material, is expensive due to its scarcity and has poor stability due to its poor resistance to corrosion from I_3^- in the electrolyte. This increases the cost of DSSCs and shortens their lifespan. As a result, several approaches such as elemental doping and developing Pt-based nanocomposites with comparable electrical conductivity and electrocatalytic activity, have been employed to improve device performance and stability.

Despite the above-mentioned efforts, the PCE and sustainability of TiO_2- and Pt-based DSSCs have continued to be low. As a result, this has necessitated the development of TiO_2- and Pt-free semiconducting materials, such as metal oxides, metal chalcogenides and perovskites, with comparable photovoltaic performance and high stability. However, on their own, these semiconducting materials tend to aggregate, giving rise to relatively low electrical conductivity and poor electrocatalytic activity, which reduces device performance. Therefore, these semiconducting materials have been recently integrated with highly conductive and sustainable carbon-based materials, particularly rGO, which is dispersible and compatible with low-cost solution synthesis. This also benefits from the advantages of rGO, such as its large specific surface area for more dye adsorption; wide and intense visible region absorption spectrum for more light absorption; high electrical conductivity for rapid electron transport with low recombination; high electrocatalytic activity for speeding up I_3^- reduction; excellent stability for prolonging device lifespan; and low-costs for reducing device cost.

From the reviewed recent studies, the use of rGO-based composites in devices based on the I^-/I_3^- redox couple and N719 dye has led to the fabrication of TiO_2-free DSSCs with an optimum PCE of ~10%, as well as Pt-free devices with a best PCE of ~12%, i.e., reaching up to ~66 and 80% of the PCE of current state-of-the-art DSSCs based on TiO_2 and Pt electrodes. Hence, the continuous optimization of parameters in future

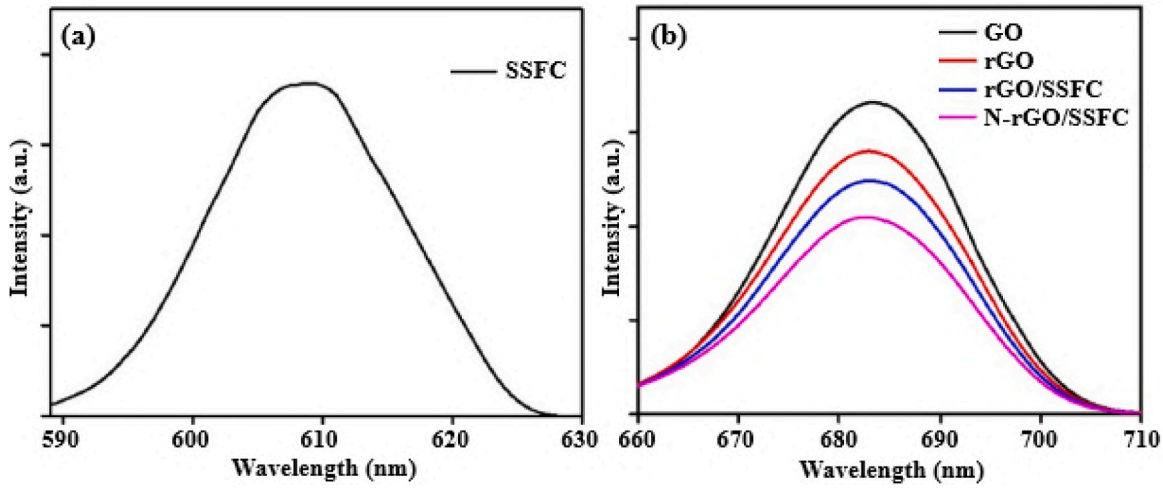

Fig. 12. PL spectra of (a) SSFC, and (b) GO, rGO, rGO/SSFC and N-rGO/SSFC. Adapted under a Creative Commons license [209], Copyright (2023), open access.

research, through approaches such as developing novel carbon-based nanocomposites, while also avoiding the dependence on scarce and costly traditional materials, has the potential to bridge the gap between emerging and traditional nanomaterials. This, if done, can conceivably lead to the development of next-generation DSSCs with a capacity to surpass the current optimum DSSC PCE (~15.2%) and approach the performance of crystalline silicon solar cells. This ultimately opens up the avenues for the commercialization of low-cost, efficient and sustainable devices. Therefore, this review has highlighted the recent progress in DSSC performance and sustainability achieved over the last five-year period (2020–2024) by fabricating TiO_2- and Pt-free electrodes, through incorporating rGO into semiconducting metal oxides, metal chalcogenides and perovskites. This is envisaged to contribute by helping to alleviate the current global issues, including the increasing energy demand, depletion of traditional energy sources, environmental pollution, global warming and climate change, through promoting the use of solar energy, a renewable energy source, which is abundant in nature, cost-effective and environmentally friendly.

CRediT authorship contribution statement

Conceptualization, E.M., E.T.M., C.M.M., T.S.S., A.Y. and D.P.; Writing – original draft, E.M., E.T.M., C.M.M., T.S.S., A.Y. and D.P.; Review and editing, E.M., E.T.M., C.M.M., T.S.S., A.Y. and D.P.

Declaration of Competing Interest

The authors declare that they have no known competing financial interests or personal relationships that could have appeared to influence the work reported in this paper.

Acknowledgements

This study was supported by Bindura University of Science Education, Faculty of Engineering and the Built Environment at University of the Witwatersrand, Botswana International University of Science and Technology, Wilfrid Laurier University, Ankara Yildirim Beyazit University, and the National Institute of Metrological Research (INRiM). Diego Pugliese acknowledges the support from the European Union - NextGenerationEU under the National Recovery and Resilience Plan (NRRP), Mission 04 Component 2 Investment 3.1 | Project Code: IR0000027 - CUP: B33C22000710006 - iENTRANCE@ENL: Infrastructure for Energy TRAnsition aNd Circular Economy @EuroNanoLab.

References

[1] W.U.H. Shah, G. Hao, H. Yan, N. Zhu, R. Yasmeen, G. Dincă, Role of renewable, non-renewable energy consumption and carbon emission in energy efficiency and productivity change: evidence from G20 economies, Geosci. Front. 15 (2024) 101631.
[2] M.K.G. Deshmukh, M. Sameeroddin, D. Abdul, M.A. Sattar, Renewable energy in the 21st century: a review, Mater. Today.: Proc. 80 (2023) 1756–1759.
[3] K. Farhana, A.S.F. Mahamude, K. Kadirgama, Comparing hydrogen fuel cost of production from various sources - a competitive analysis, Energy Convers. Manag. 302 (2024) 118088.
[4] L. Pang, L. Liu, X. Zhou, M. Hafeez, S. Ullah, M.T. Sohail, How does natural resource depletion affect energy security risk? New insights from major energy-consuming countries, Energy Strat. Rev. 54 (2024) 101460.
[5] N. Shahzad, Lutfullah, T. Perveen, D. Pugliese, S. Haq, N. Fatima, S.M. Salman, A. Tagliaferro, M.I. Shahzad, Counter electrode materials based on carbon nanotubes for dye-sensitized solar cells, Renew. Sustain. Energy Rev. 159 (2022) 112196.
[6] G. Mutezo, J. Mulopo, A review of Africa's transition from fossil fuels to renewable energy using circular economy principles, Renew. Sustain. Energy Rev. 137 (2021) 110609.
[7] J. Conradie, Effective dyes for DSSCs–Important experimental and calculated parameters, Energy Nexus 13 (2024) 100282.
[8] K. Prajapat, M. Dhonde, K. Sahu, P. Bhojane, V.V.S. Murty, P.M. Shirage, The evolution of organic materials for efficient dye-sensitized solar cells, J. Photochem. Photobiol., C: Photochem. Rev. 55 (2023) 100586.
[9] K. Ahmad, H. Kim, A brief overview of electrode materials for hydrazine sensors and dye-sensitized solar cells, Microchem. J. 186 (2023) 108317.
[10] I. Karakurt, G. Aydin, Development of regression models to forecast the CO_2 emissions from fossil fuels in the BRICS and MINT countries, Energy 263 (2023) 125650.
[11] F. Chien, How renewable energy and non-renewable energy affect environmental excellence in N-11 economies? Renew. Energy 196 (2022) 526–534.
[12] M.Y. Ong, S. Nomanbhay, F. Kusumo, P.L. Show, Application of microwave plasma technology to convert carbon dioxide (CO_2) into high value products: a review, J. Clean. Prod. 336 (2022) 130447.
[13] P.M.B. Abrasaldo, S.J. Zarrouk, A.W. Kempa-Liehr, A systematic review of data analytics applications in above-ground geothermal energy operations, Renew. Sustain. Energy Rev. 189 (2024) 113998.
[14] G.M. Idroes, I. Hardi, I.S. Hilal, R.T. Utami, T.R. Noviandy, R. Idroes, Economic growth and environmental impact: assessing the role of geothermal energy in developing and developed countries, Innov. Green. Dev. 3 (2024) 100144.
[15] Y. Liu, Y. Huang, Assessing the interrelationship between fossil fuels resources and the biomass energy market for achieving a sustainable and green economy, Resour. Policy 88 (2024) 104397.
[16] T. Hai, M.A. Ali, A. Alizadeh, S.F. Almojil, A.I. Almohana, A.F. Alali, Reduction in environmental CO_2 by utilization of optimized energy scheme for power and fresh water generations based on different uses of biomass energy, Chemosphere 319 (2023) 137847.
[17] J.V. Ringwood, S. Zhan, N. Faedo, Empowering wave energy with control technology: possibilities and pitfalls, Annu. Rev. Control 55 (2023) 18–44.
[18] G. Yao, Z. Luo, Z. Lu, M. Wang, J. Shang, J.M. Guerrerob, Unlocking the potential of wave energy conversion: a comprehensive evaluation of advanced maximum power point tracking techniques and hybrid strategies for sustainable energy harvesting, Renew. Sustain. Energy Rev. 185 (2023) 113599.
[19] Z. Nizamani, A.K. Muhammad, M.O.A. Ali, M.A. Wahab, A. Nakayama, M. M. Ahmed, Renewable wind energy resources in offshore low wind speeds regions near the equator: a review, Ocean Eng. 311 (2024) 118834.
[20] A. Martinez, G. Iglesias, Global wind energy resources decline under climate change, Energy 288 (2024) 129765.
[21] T. Falope, L. Lao, D. Hanak, D. Huo, Hybrid energy system integration and management for solar energy: a review, Energy Convers. Manag.: X 21 (2024) 100527.
[22] H.H. Pourasl, R.V. Barenji, V.M. Khojastehnezhad, Solar energy status in the world: a comprehensive review, Energy Rep. 10 (2023) 3474–3493.
[23] L. Li, B. Lu, W. Xu, C. Wang, J. Wu, D. Tan, Dynamic behaviors of multiphase vortex-induced vibration for hydropower energy conversion, Energy 308 (2024) 132897.
[24] Q. Tan, Z. Zhang, X. Wen, G. Fang, S. Xu, Z. Nie, Y. Wang, Risk control of hydropower-photovoltaic multi-energy complementary scheduling based on energy storage allocation, Appl. Energy 358 (2024) 122610.
[25] A. Ashok, T. Raguram, R.J. Beula, G. Gopinath, S. Ayyasamy, A. Abiram, A. Mohan, C.B. Beril Ramolin, B. Vidhya, Synergistic effects of Co-Mn co-doping on the structural and optical properties of TiO_2 nanospheres: dual functions for DSSC photoanodes and degradation photocatalyst, J. Alloy. Compd. 1005 (2024) 176024.
[26] M. Gokulnaath, V.S. Manikandan, S. Muthu Mariappan, S. Harish, J. Archana, M. Navaneethan, Tailoring the band edge potential in Y^{3+} doped $BaSnO_3$ photoanode in dye sensitized solar cell applications, J. Phys. Chem. Solids 179 (2023) 111367.
[27] J. Raveena, R.R. Chandrapal, G. Bakiyaraj, V.S. Manikandan, S. Athitya, J. Archana, M. Navaneethan, Synergetic effect of 2D/2D Co-SnS_2 with reduced graphene oxide heterostructure for Pt-free counter electrode, Mater. Today Commun. 34 (2023) 105204.
[28] L. Sivasankaran, S.C. Pradhan, R.K. Mishra, S. Soman, A. Ajayaghosh, Role of alkyl groups regulating recombination and mass transport at cobalt electrolyte-dye interface in dye sensitized solar cells, Sol. Energy 236 (2022) 182–194.
[29] F. Yuliasari, A. Aprilia, R. Hidayat, Improved dye-sensitized solar cell performance with hedgehog-like shaped ZnO nanorods grown using ZnO nanoparticles seed layer, Mater. Today.: Proc. 52 (2022) 248–251.
[30] L.L. Larina, O. Omelianovych, V.-D. Dao, K. Pyo, D. Lee, H.-S. Choi, Energy band alignment at the heterointerface between a nanostructured TiO_2 layer and $Au_{22}(SG)_{18}$ clusters: relevance to metal-cluster-sensitized solar cells, Nanoscale 13 (2021) 175–184.
[31] M. Matsumura, S. Matsudaira, H. Tsubomura, Dye sensitization and surface structures of semiconductor electrodes, Ind. Eng. Chem. Prod. Res. Dev. 19 (1980) 415–421.
[32] B. O'Regan, M. Grätzel, A low-cost, high-efficiency solar cell based on dye-sensitized colloidal TiO_2 films, Nature 353 (1991) 737–740.
[33] B.K. Korir, J.K. Kibet, S.M. Ngari, A review on the current status of dye-sensitized solar cells: toward sustainable energy, Energy Sci. Eng. 12 (2024) 3188–3226.
[34] P.S. Saud, A. Bist, A.A. Kim, A. Yousef, A. Abutaleb, M. Park, S.-J. Park, B. Pant, Dye-sensitized solar cells: fundamentals, recent progress, and Optoelectrical properties improvement strategies, Opt. Mater. 150 (2024) 115242.
[35] T.M.W.J. Bandara, S.M.S. Gunathilake, M.A.K.L. Dissanayake, B.M.K. Pemasiri, I. Albinsson, B.-E. Mellander, A review of the development of graphene-incorporated dye-sensitized solar cells, 30 (2024) 6789–6809.
[36] P. Chawla, M. Tripathi, Novel improvements in the sensitizers of dye-sensitized solar cells for enhancement in efficiency - a review, Int. J. Energy Res. 39 (2015) 1579–1720.
[37] M.-E. Yeoh, K.-Y. Chan, Recent advances in photo-anode for dye-sensitized solar cells: a review, Int. J. Energy Res. 41 (2017) 2439–2595.

[38] N. Tomar, V.S. Dhaka, P.K. Surolia, A brief review on carbon nanomaterial counter electrodes for N719 based dye-sensitized solar cells, Mater. Today.: Proc. (2021) 2975–2978.

[39] J. Wu, Z. Lan, J. Lin, M. Huang, Y. Huang, L. Fan, G. Luo, Electrolytes in dye-sensitized solar cells, Chem. Rev. 115 (2015) 2136–2173.

[40] Y. Ren, D. Zhang, J. Suo, Y. Cao, F.T. Eickemeyer, N. Vlachopoulos, S. M. Zakeeruddin, A. Hagfeldt, M. Grätzel, Hydroxamic acid pre-adsorption raises the efficiency of cosensitized solar cells, Nature 613 (2023) 60–65.

[41] D. Devadiga, M. Selvakumar, P. Shetty, M.S. Santosh, Dye-sensitized solar cell for indoor applications: a mini-review, J. Electron. Mater. 50 (2021) 3187–3206.

[42] M. Chinnarani, K.M. Prabu, S. Suresh, Plasmonic silver loaded anatase titanium dioxide nanospheres photoanode for dye-sensitized solar cell, Results Chem. 5 (2023) 100835.

[43] M. Kandasamy, A.H. Seikh, S. Suresh, A. Kumar, A. Husain, P. Vijayakumar, T. T. Dele-Afolabi, N. Pugazhenthiran, S. Murugesan, M.N.M. Ansari, Fabrication of ternary zinc-nickel-copper oxide microsphere nanocomposite photoanode material for boosting dye-sensitized solar cell efficiency, J. Alloy. Compd. 1000 (2024) 175039.

[44] R. Senthamarai, V. Madurai Ramakrishnan, P. Murugan, A. Ponnusamy Munusamy, S. Kulandhaivel, Synthesis and characterization of nickel doped TiO_2 nanoparticles by green method and its performance as dye-sensitized solar cells photoanodes, Int. J. Energy Res. 46 (2022) 7749–7757.

[45] National Renewable Energy Laboratory, Best research-cell efficiency chart. ⟨https://www.nrel.gov/pv/assets/pdfs/best-research-cell-efficiencies.pdf⟩, 2024 (accessed 01 September 2024).

[46] A. Rathika, I.John Peter, V. Ragavendran, J. Mayandi, P. Nithiananthi, MWCNT supported CuS/ZrS_3 composite: a versatile multifunctional catalyst for dye-sensitized solar cells, water splitting, and supercapacitors, Electrochim. Acta 477 (2024) 143746.

[47] Y. Gao, W. Liao, W. Wang, X. Zuo, Q. Yang, H. Tang, S. Jin, G. Li, $FeS_2/FeCoS_2$ nanoparticles/reduced graphene oxide interfacial composite structure as highly reactive counter electrodes in dye-sensitized solar cells, J. Mater. Sci.: Mater. Electron. 32 (2021) 8226–8236.

[48] Y. Areerob, C. Hamontree, P. Sricharoen, N. Limchoowong, S. Laksee, W.-C. Oh, K. Pattarith, Novel gamma-irradiated chitosan-doped reduced graphene-$CuInS_2$ composites as counter electrodes for dye-sensitized solar cells, RSC Adv. 12 (2022) 15427–15434.

[49] X. Wang, B. Zhao, W. Kan, Y. Xie, K. Pan, Review on low-cost counter electrode materials for dye-sensitized solar cells: effective strategy to improve photovoltaic performance, Adv. Mater. Interfaces 9 (2022) 2101229.

[50] X. Yao, B. He, L. Cui, J. Ti, H. Chen, Y. Duan, Q. Tang, Polypyrrole-molybdenum sulfide complex as an efficient and transparent catalytic electrode for bifacial dye-sensitized solar cells, Catal. Commun. 163 (2022) 106403.

[51] O.H. Al-Zoubi, E.A.M. Saleh, A.N.A. Saieed, B.D. Olegovich, E.R. Alwaily, A. Alawadi, M. Talal, Y.F. Mustafa, Platinum-free counter electrode based on $ZnCo_2O_4$@NiO core-shell nanostructures in dye-sensitized solar cells, Mater. Sci. Semicond. Process. 174 (2024) 108234.

[52] A. Anand, S. Mittal, V. Leeladevi, D. De, Nanoflower shaped ZnO photoanode and natural dye sensitizer based solar cell fabrication, Mater. Today.: Proc. 72 (2023) 227–231.

[53] E.S. Sowbakkiyavathi, V. Murugadoss, S.P. Rajendra, M.S. AlSalhi, P. Dhandapani, S. Angaiah, Nickel selenide embedded polyaniline nanofibers as a counter electrode for high-performance dye-sensitized solar cell, J. Mol. Struct. 1305 (2024) 137735.

[54] P.P. Sanap, S.P. Gupta, S.S. Kahandal, J.L. Gunjakar, C.D. Lokhande, B. R. Sankapal, Z. Said, R.N. Bulakhe, J.M. Kim, A.B. Bhalerao, Exploring vanadium-chalcogenides toward solar cell application: a review, J. Ind. Eng. Chem. 129 (2024) 124–142.

[55] S. Ndlovu, E. Muchuweni, V.O. Nyamori, Effect of ball milling time on $Sr_{0.7}Sm_{0.3}Fe_{0.4}Co_{0.6}O_{2.65}$ perovskites and their application as semiconductor layers in dye-sensitized solar cells, Heliyon 10 (2024) e33347.

[56] K.B. Bhojanaa, A. Soundarya Mary, K.S.S. Devi, N. Pavithra, A. Pandikumar, Account of structural, theoretical, and photovoltaic properties of ABO_3 oxide perovskites photoanode-based dye-sensitized solar cells, Sol. RRL 6 (2022) 2100792.

[57] S. Upadhyay, S. Narendhiran, M. Balachandran, Exploring the role of structurally modified molybdenum disulfide composites with Prussian blue analogues as counter electrode catalysts for bifacial dye-sensitized solar cells, Sol. Energy 282 (2024) 112906.

[58] N.S. Samsi, N.A.S. Affendi, M.K. Yaakob, M.F.M. Taib, A. Lepit, O.H. Hassan, M.Z. A. Yahya, A.M.M. Ali, Characteristics of electron transport study of composited graphene-zinc oxide thin film photoanode for dye-sensitized solar cells, Solid State Phenom. 307 (2020) 185–191.

[59] M.J. Ju, I.T. Choi, M. Zhong, K. Lim, J. Ko, J. Mohin, M. Lamson, T. Kowalewski, K. Matyjaszewski, H.K. Kim, Copolymer-templated nitrogen-enriched nanocarbons as a low charge-transfer resistance and highly stable alternative to platinum cathodes in dye-sensitized solar cells, J. Mater. Chem. A 3 (2015) 4413–4419.

[60] M. Aftabuzzaman, C. Lu, H.K. Kim, Recent progress on nanostructured carbon-based counter/back electrodes for high-performance dye-sensitized and perovskite solar cells, Nanoscale 12 (2020) 17590–17648.

[61] M. Aftabuzzaman, M.S. Ahmed, K. Matyjaszewski, H.K. Kim, Nanocrystal co-existed highly dense atomically disperse Pt@3D-hierarchical porous carbon electrocatalysts for tri-iodide and oxygen reduction reactions, Chem. Eng. J. 446 (2022) 137249.

[62] H.-L.T. Dang, N.A. Tran, V.-D. Dao, N.H. Vu, D.V. Quang, H.H.T. Vu, T. H. Nguyen, T.-D. Pham, X.-C. Hoang, H.T. Nguyen, P.A. Tuan, Carbon nanotubes-ruthenium as an outstanding catalyst for triiodide ions reduction, Synth. Met. 260 (2020) 116299.

[63] V.-D. Dao, Bimetallic PtSe nanoparticles incorporating with reduced graphene oxide as efficient and durable electrode materials for liquid-junction photovoltaic devices, Mater. Today Energy 16 (2020) 100384.

[64] E. Muchuweni, B.S. Martincigh, V.O. Nyamori, Recent advances in graphene-based materials for dye-sensitized solar cell fabrication, RSC Adv. 10 (2020) 44453–44469.

[65] S.Rubesh Ashok Kumar, D. Vasvini Mary, G.A. Suganya Josephine, A. Riswan Ahamed Mohamed, Graphene/GO/rGO based nanocomposites: emerging energy and environmental application–review, Hybrid. Adv. 5 (2024) 100168.

[66] P. Jain, R.S. Rajput, S. Kumar, A. Sharma, A. Jain, B.J. Bora, P. Sharma, R. Kumar, M. Shahid, A.A. Rajhi, M. Alsubih, M.A. Shah, A. Bhowmik, Recent advances in graphene-enabled materials for photovoltaic applications: a comprehensive review, ACS Omega 9 (2024) 12403–12425.

[67] H. Su, Y.H. Hu, 3D graphene: synthesis, properties, and solar cell applications, Chem. Commun. 59 (2023) 6660–6673.

[68] A.S. Joshi, E. Elamurugu, S. Leela, Impact of graphene oxide (GO) and reduced graphene oxide (rGO) on the TiO_2 thin film composite (TiO_2:GO/rGO) photoanodes, Chem. Phys. Impact 9 (2024) 100667.

[69] K.M. Alanezi, I. Ahmad, S. AlFaify, I. Ali, A. Mohammad, M.S. Jabir, H. Majdi, F. M. Almutairi, A review of advanced heteroatom-doped graphene and its derivatives materials for photocatalytic applications, J. Ind. Eng. Chem. (2024), https://doi.org/10.1016/j.jiec.2024.08.029.

[70] N.H. Hieu, H.H. Dat, L.T.T. Nghia, N.M. Dat, L.N. Phat, N.T. Tinh, P.T. Khang, N. T. Hoang, M.T. Phong, Synthesis of nitrogen and sulfur co-doped reduced graphene oxide by hydrothermal method for fabrication of cathodes in dye-sensitized solar cells, FlatChem 31 (2022) 100318.

[71] S. Kamesh, S. Athithya, S. Harish, M. Shimomura, M. Navaneethan, J. Archana, Nitrogen-doped reduced graphene oxide enfolded zinc cobaltite micro flowers as efficient triiodide reduction for a platinum-free counter electrode in dye-sensitized solar cell applications, Electrochim. Acta 475 (2024) 143262.

[72] S. Santra, A. Bose, K. Mitra, A. Adalder, Exploring two decades of graphene: the jack of all trades, Appl. Mater. Today 36 (2024) 102066.

[73] E. Muchuweni, E.T. Mombeshora, C.M. Muiva, T.S. Sathiaraj, Towards high-performance lithium-ion batteries by introducing graphene-based materials into $LiFePO_4$ cathodes: a review, Nano Trends 6 (2024) 100034.

[74] A. Agrawal, Top-down strategies for achieving high-quality graphene: recent advancements, J. Ind. Eng. Chem. (2024), https://doi.org/10.1016/j.jiec.2024.07.053.

[75] Y. Wen, H. Liu, X. Jiang, Preparation of graphene by exfoliation and its application in lithium-ion batteries, J. Alloy. Compd. 961 (2023) 170885.

[76] A. Rasyotra, A. Thakur, B. Gaykwad, S. Chakrabarty, I. Bayad, J. Parikh, K. Jasuja, A review of low-cost approaches to synthesize graphene and its functional composites, J. Mater. Sci. 58 (2023) 4359–4383.

[77] K.S. Obayomi, S.Y. Lau, I.E. Mayowa, M.K. Danquah, J. Zhang, T. Chiong, L. Meunier, M.M. Rahman, Recent advances in graphene-derived materials for biomedical waste treatment, J. Water Process Eng. 51 (2023) 103440.

[78] P.M. Biranje, A.W. Patwardhan, J.B. Joshi, K. Dasgupta, Exfoliated graphene and its derivatives from liquid phase and their role in performance enhancement of epoxy matrix composite, Compos. Part A: Appl. Sci. Manuf. 156 (2022) 106886.

[79] L. Wang, B. Xin, A. Elsukova, P. Eklund, N. Solin, Mechanochemical formation of protein nanofibril: graphene nanoplatelet hybrids and their thermoelectric properties, ACS Sustain. Chem. Eng. 8 (2020) 17368–17378.

[80] C. Marchi, H.A. Loh, F. Lissandrello, A. Lucotti, K.A. Sierros, L. Magagnin, Biocompatible rapid few-layers-graphene synthesis in aqueous lignin solutions, Carbon Trends 7 (2022) 100169.

[81] F.J. Sonia, M. Aslam, A. Mukhopadhyay, Understanding the processing-structure-performance relationship of graphene and its variants as anode material for Li-ion batteries: a critical review, Carbon 156 (2020) 130–165.

[82] E. Igman, O. Bayram, A. Mavi, U.C. Hasar, O. Simsek, Photovoltaic performance of non-covalent functionalized single-layer graphene in dye-sensitized solar cells (DSSCs), J. Mater. Sci. 56 (2021) 4184–4196.

[83] A.K. Worku, D.W. Ayele, Recent advances of graphene-based materials for emerging technologies, Results Chem. 5 (2023) 100971.

[84] R. Goodrum, H. Weldekidan, H. Li, A.K. Mohanty, M. Misra, Graphene-based nanostructures from green processes and their applications in biomedical sensors, Adv. Ind. Eng. Polym. Res. 7 (2024) 37–53.

[85] J. Singh, N. Jindal, V. Kumar, K. Singh, Role of green chemistry in synthesis and modification of graphene oxide and its application: a review study, Chem. Phys. Impact 6 (2023) 100185.

[86] J. Nam, J. Yang, Y. Zhao, K.S. Kim, Chemical vapor deposition of graphene and its characterizations and applications, Curr. Appl. Phys. 61 (2024) 55–70.

[87] H. Kang, P. Tang, H. Shu, Y. Zhang, Y. Liang, J. Li, Z. Chen, Y. Sui, S. Hu, S. Wang, S. Zhao, X. Zhang, C. Jiang, Y. Chen, Z. Xue, M. Zhang, D. Jiang, G. Yu, S. Peng, Z. Jin, X. Liu, Epitaxial growth of wafer scale antioxidant single-crystal graphene on twinned Pt(111), Carbon 181 (2021) 225–233.

[88] M.G. Choi, S. Park, H. Lee, S. Kim, Correlating surface structures and nanoscale friction of CVD multi-layered graphene, Appl. Surf. Sci. 584 (2022) 152572.

[89] W. Lee, G. Lim, S.H. Ko, Significant thermoelectric conversion efficiency enhancement of single layer graphene with substitutional silicon dopants, Nano Energy 87 (2021) 106188.

[90] H.J. Hwang, S.-Y. Kim, S.K. Lee, B.H. Lee, Large scale graphene thermoelectric device with high power factor using gradient doping profile, Carbon 201 (2023) 467–472.

[91] M. Schrade, W. Xing, K. Thorshaug, B.D. Belle, Centimeter-sized monolayer CVD graphene with high power factor for scalable thermoelectric applications, ACS Appl. Electron. Mater. 4 (2022) 1506–1510.

[92] E. Muchuweni, E.T. Mombeshora, B.S. Martincigh, V.O. Nyamori, Photovoltaics: background and novel carbon-based materials for third-generation solar cells, in: N.V. Kulkarni, B.I. Kharissov (Eds.), Handbook of Emerging Materials for Sustainable Energy, Elsevier, New York, 2024, pp. 197–235.

[93] A.A. Qureshi, S. Javed, H.M.A. Javed, A. Akram, M.S. Mustafa, U. Ali, M.Z. Nisar, Facile formation of SnO_2–TiO_2 based photoanode and Fe_3O_4@rGO based counter electrode for efficient dye-sensitized solar cells, Mater. Sci. Semicond. Process. 123 (2021) 105545.

[94] S. Hussain, S.S. Maktedar, Structural, functional and mechanical performance of advanced graphene-based composite hydrogels, Results Chem. 6 (2023) 101029.

[95] D. Singh, V. Shukla, R. Ahuja, Optical excitations and thermoelectric properties of two-dimensional holey graphene, Phys. Rev. B 102 (2020) 075444.

[96] Z. Liu, R. Navik, H. Tan, Q. Xiang, Wahyudiono, M. Goto, R.M. Ibarra, Y. Zhao, Graphene-based materials prepared by supercritical fluid technology and its application in energy storage, J. Supercrit. Fluids 188 (2022) 105672.

[97] H. Aghamohammadi, N. Hassanzadeh, R. Eslami-Farsani, A review study on the recent advances in developing the heteroatom-doped graphene and porous graphene as superior anode materials for Li-ion batteries, Ceram. Int. 47 (2021) 22269–22301.

[98] P. Sehrawat, A. Shabir, Abid, C.M. Julien, S.S. Islam, Recent trends in silicon/graphene nanocomposite anodes for lithium-ion batteries, J. Power Sources 501 (2021) 229709.

[99] T.A. Amollo, Metallic nanoparticles and hybrids of metallic nanoparticles/graphene nanomaterials for enhanced photon harvesting and charge transport in polymer and dye sensitized solar cells, Heliyon 10 (2024) e26401.

[100] A. Ahmed, A. Singh, S.-J. Young, V. Gupta, M. Singh, S. Arya, Synthesis techniques and advances in sensing applications of reduced graphene oxide (rGO) composites: a review, Compos. Part A: Appl. Sci. Manuf. 165 (2023) 107373.

[101] P. Majumder, R. Gangopadhyay, Evolution of graphene oxide (GO)-based nanohybrid materials with diverse compositions: an overview, RSC Adv. 12 (2022) 5686–5719.

[102] A. Razaq, F. Bibi, X. Zheng, R. Papadakis, S.H.M. Jafri, H. Li, Review on graphene-, graphene oxide-, reduced graphene oxide-based flexible composites: from fabrication to applications, Materials 15 (2022) 1012.

[103] N.C. Joshi, P. Gururani, Advances of graphene oxide based nanocomposite materials in the treatment of wastewater containing heavy metal ions and dyes, Curr. Res. Green. Sustain. Chem. 5 (2022) 100306.

[104] A.S. Joshi, S. Leela, E. Elamurugu, T. Deeparani, Influence of GO and rGO on the structural and optical properties of ZnO photoelectrodes for energy harvesting applications, Mater. Sci. Eng.: B 299 (2024) 116938.

[105] E. Muchuweni, E.T. Mombeshora, C.M. Muiva, T.S. Sathiaraj, Lithium-ion batteries: recent progress in improving the cycling and rate performances of transition metal oxide anodes by incorporating graphene-based materials, J. Energy Storage 73 (2023) 109013.

[106] N.P.D. Ngidi, E. Muchuweni, V.O. Nyamori, Dual heteroatom-doped reduced graphene oxide and its application in dye-sensitized solar cells, Opt. Mater. 122 (2021) 111689.

[107] R. Sharma, H. Kumar, D. Yadav, C. Saini, R. Kumari, G. Kumar, A.B. Kajjam, V. Pandit, M. Ayoub, Saloni, Y. Deswal, A.K. Sharma, Synergistic advancements in nanocomposite design: harnessing the potential of mixed metal oxide/reduced graphene oxide nanocomposites for multifunctional applications, J. Energy Storage 93 (2024) 112317.

[108] M. Mirzaei, M.B. Gholivand, Synthesis of ruthenium sulfide nanoparticles decorated on reduced graphene oxide/multi-walled carbon nanotubes as a catalytic counter electrode for dye-sensitized solar cells exceeding 13 % efficiency, Sol. Energy 242 (2022) 212–224.

[109] F. Kabir, S. Manir, M.M.H. Bhuiyan, S. Aftab, H. Ghanbari, A. Hasani, M. Fawzy, G.L.T. De Silva, M.R. Mohammadzadeh, R. Ahmadi, A. Abnavi, A.M. Askar, M. M. Adachi, Instability of dye-sensitized solar cells using natural dyes and approaches to improving stability – an overview, Sustain. Energy Technol. Assess. 52 (2022) 102196.

[110] W.N. Bahutair, A. Alhajar, A.A. Othman, M. Tawalbeh, The role of MXenes and MXene composites in enhancing dye-sensitized solar cells characteristics, Process Saf. Environ. Prot. 191 (2024) 490–504.

[111] B. Aljafari, S. James, A. Sorrentino, S. Anandan, Nanostructured g-C_3N_4-decorated TiO_2 for superior photoanode performance in dye-sensitized solar cells, Inorg. Chem. Commun. 159 (2024) 111737.

[112] P. Ningthoukhongjam, P.Mathan Kumar, M. Bhagavathiachari, R.G. Nair, Multiphasic titania photoanode: a facile phase assisted approach to enhance the photoelectrochemical and photovoltaic performance, Opt. Mater. 156 (2024) 115995.

[113] M. Ayaz, M. Hijji, A.S. Alatawi, M.A. Namazi, M.I.M. Ershath, Improving charge transfer properties and solar cell performance by In-doped TiO_2 as an efficient photoanode for dye-sensitized solar cells (DSSCs), J. Phys. Chem. Solids 188 (2024) 111913.

[114] W. Moloto, P.J. Mafa, P. Mbule, E. Nxumalo, B. Ntsendwana, Photoinduced electrochemical effect of porous BiPOM on TiO_2 photoanode performance for dye-sensitized solar cells application, Mater. Today Commun. 30 (2022) 103001.

[115] S. Vibavakumar, K.D. Nisha, J. Archana, M. Navaneethan, S. Harish, Synergistic effect and enhanced charge transfer in Nb_2O_5-rGO/TiO_2 photoanode for dye-sensitized solar cells, Sol. Energy 271 (2024) 112398.

[116] G.T. Tractz, F.S. da Luz, S.R.M. Antunes, E. do Prado Banczek, M.T. da Cunha, P. R.P. Rodrigues, Nb_2O_5 synthesis and characterization by Pechini method to the application as electron transport material in a solar device, Sol. Energy 216 (2021) 1–6.

[117] H. Niu, X. Yao, S. Luo, Y. Xie, T. Li, W. Chen, L. Wan, H. Wang, R. Zhou, Y. Du, L. Hu, J. Xu, Combination of multiple routes to enhance DSSC performance: flower-like structure of SnO_2 as photoanode and modification with Ag nanoparticle, Mater. Sci. Semicond. Process. 177 (2024) 108363.

[118] R. Vasanthapriya, N. Neelakandeswari, K. Uthayarani, M. Chitra, Parthenium hysterophorous flower template assisted SnO_2 nanostructure as photoanode for dye sensitized solar cell, Chem. Phys. Impact 7 (2023) 100308.

[119] M. Abrari, M. Ahmadi, H.M. Chenari, M. Ghanaatshoar, Investigating the effect of ZrO_2 nanofibers in ZnO-based photoanodes to increase dye-sensitized solar cells (DSSC) efficiency: inspecting the porosity and charge transfer properties in ZnO/ZrO_2 nanocomposite photoanode, Opt. Mater. 147 (2024) 114690.

[120] P. Nandi, D. Das, Morphological variations of ZnO nanostructures and its influence on the photovoltaic performance when used as photoanodes in dye sensitized solar cells, Sol. Energy Mater. Sol. Cells 243 (2022) 111811.

[121] A. Tiwari, S. Singh, P. Srivastava, Exploring the potential of potato starch-capped TiO_2 nanoparticles for DSSC photoanodes, Results Opt. 15 (2024) 100630.

[122] E.S. Esakki, G. Deepa, P. Vivek, S.M. Sundar, Investigation of TiO_2 as photoanode for solar cell application, Solid State Commun. 371 (2023) 115266.

[123] F. Mujtahid, P.L. Gareso, B. Armynah, D. Tahir, Review effect of various types of dyes and structures in supporting performance of dye-sensitized solar cell TiO_2-based nanocomposites, Int. J. Energy Res. 46 (2022) 726–742.

[124] J.-H. Bae, S.-B. Do, S.-H. Cho, K.-M. Lee, S.-E. Lee, T.-O. Kim, TiO_2 treatment using ultrasonication for bubble cavitation generation and efficiency assessment of a dye-sensitized solar cell, Ultrason. Sonochem. 83 (2022) 105933.

[125] L. Wei, X. Xu, L. Zhao, J. Liu, R. Wang, X. Zhang, Design and fabrication of layered TiO_2/rGO composited photoanode and its photovoltaic performance regulation for dye-sensitized solar cells, Opt. Mater. 154 (2024) 115709.

[126] I. Ahmad, R. Jafer, S.M. Abbas, N. Ahmad, A.-U. Rehman, J. Iqbal, S. Bashir, A. A. Melaibari, M.H. Khan, Improving energy harvesting efficiency of dye sensitized solar cell by using cobalt-rGO co-doped TiO_2 photoanode, J. Alloy. Compd. 891 (2022) 162040.

[127] M. Irfan, M.I. Khan, Ikram-ul-haq, M. Amami, R. Ahson, E.A. Alabbad, Effect of Fe ions beam on the structural, optical, photovoltaic properties of TiO_2 based dye-sensitized solar cells, Opt. Mater. 123 (2022) 111794.

[128] L.O.A. Salim, M.Z. Muzakkar, A. Zaeni, M. Maulidiyah, M. Nurdin, S.N. Sadikin, J. Ridwan, A.A. Umar, Improved photoactivity of TiO_2 photoanode of dye-sensitized solar cells by sulfur doping, J. Phys. Chem. Solids 175 (2023) 111224.

[129] N.H. Shamsudin, S. Shafie, M.Z.A. Ab Kadir, F. Ahmad, Y. Sulaiman, S.A. M. Chachuli, M.C. Razali, Flexible back-illuminated dye sensitised solar cells (DSSCs) with titanium dioxide/silver nanoparticles composite photoanode for improvement of power conversion efficiency, Optik 272 (2023) 170237.

[130] B.T. Huy, D.H. Kwon, S.-S. Lee, V.-D. Dao, H.B. Truong, Y.-I. Lee, Optical properties of Sr_2YF_7 material doped with Yb^{3+}, Er^{3+}, and Eu^{3+} ions for solar cell application, J. Alloy. Compd. 897 (2022) 163189.

[131] M. Chinnarani, S. Suresh, K.M. Prabu, M. Kandasamy, N. Pugazhenthiran, Facile synthesis of reduced graphene oxide and graphitic carbon nitride modified titanium dioxide nanospheres for photoanode of dye-sensitized solar cell, Inorg. Chim. Acta 560 (2024) 121842.

[132] V.S. Katta, V.R. Chappidi, A. Kumar, S. Asthana, S.S.K. Raavi, Enriched visible light absorption by Au-embedded Sm^{3+} doped TiO_2 compact photoanode for enhanced dye-sensitized solar cell performance, Phys. B: Condens. Matter 652 (2023) 414621.

[133] E. Muchuweni, E.T. Mombeshora, B.S. Martincigh, V.O. Nyamori, Graphitic carbon nitride-based new-generation solar cells: critical challenges, recent breakthroughs and future prospects, Sol. Energy 239 (2022) 74–87.

[134] N.P.D. Ngidi, E. Muchuweni, V.O. Nyamori, Enhanced performance by heteroatom-doped reduced graphene oxide-TiO_2-based nanocomposites as photoanodes in dye-sensitised solar cells, Int. J. Energy Res. 46 (2022) 13670–13686.

[135] G.G. Ninan, M. Varghese, M. Balachandran, Performance of DSSC with green synthesized and thermodynamically sintered Bi-phase TiO_2 with various sensitizers, Opt. Mater. 149 (2024) 115004.

[136] V.M. Ramakrishnan, S. Pitchaiya, N. Muthukumarasamy, K. Kvamme, G. Rajesh, S. Agilan, A. Pugazhendhi, D. Velauthapillai, Performance of TiO_2 nanoparticles synthesized by microwave and solvothermal methods as photoanode in dye-sensitized solar cells (DSSC), Int. J. Hydrog. Energy 45 (2020) 27036–27046.

[137] M.N. Mustafa, Y. Sulaiman, Review on the effect of compact layers and light scattering layers on the enhancement of dye-sensitized solar cells, Sol. Energy 215 (2021) 26–43.

[138] F. Ziaeifar, A. Alizadeh, Z. Shariatinia, Dye sensitized solar cells fabricated based on nanocomposite photoanodes of TiO_2 and $AlMo_{0.5}O_3$ perovskite nanoparticles, Sol. Energy 218 (2021) 435–444.

[139] N. Sarwar, R. Ghaffar, M. Shahzad, K. Javed, M. Munam, Z. Siddiq, A. Pervez, M. Z. Khan, M. Saleem, J.-H. Koh, A. Ghaffar, Synergistic photovoltaic performance of DSSCs based on ZnO charge transport layers, counter electrodes and *C. annuum* and *T. indica* as natural dyes, Mater. Sci. Eng.: B 307 (2024) 117543.

[140] H. Esgin, Y. Caglar, M. Caglar, Photovoltaic performance and physical characterization of Cu doped ZnO nanopowders as photoanode for DSSC, J. Alloy. Compd. 890 (2022) 161848.

[141] M. Biçer, M. Gökçen, E. Orhan, Fabrication and photoanode performance of ZnO nanoflowers in ZnO-based dye-sensitized solar cells, Opt. Mater. 131 (2022) 112691.
[142] G. Deogratias, O.S. Al-Qurashi, N. Wazzan, Optical and electronic properties enhancement via chalcogenides: promising materials for DSSC applications, J. Mol. Model. 29 (2023) 86.
[143] M. Prabhu, M. Marikkannan, M.S. Pandian, P. Ramasamy, K. Ramachandra, Effect of zinc and indium doping in chalcogenide (CdS/Te) nanocomposites towards dye-sensitized solar cell applications, J. Phys. Chem. Solids 168 (2022) 110802.
[144] M. Gokulnaath, S. Athithya, V.S. Manikandan, M. Navaneethan, J. Archana, Investigating the effect of Y^{3+}/La^{3+} co-dopant on Ba site of $BaSnO_3$ as an efficient photoanode for dye sensitized solar cell application, Opt. Mater. 156 (2024) 115952.
[145] M. Rekha, R. Yadav, L. Cindrella, $Ni_{1-x}Fe_xMnO_3$ perovskite photoanodes for dye-sensitized solar cells (DSSCs), Opt. Mater. 143 (2023) 114172.
[146] A. Alizadeh, M. Roudgar-Amoli, S.-M. Bonyad-Shekalgourabi, Z. Shariatinia, M. Mahmoudi, F. Saadat, Dye sensitized solar cells go beyond using perovskite and spinel inorganic materials: a review, Renew. Sustain. Energy Rev. 157 (2022) 112047.
[147] S. Kalia, R. Kumar, R. Dhiman, R.K. Singh, Ion irradiation/implantation induced defect engineering and modification in graphene derivatives-based nanocomposites: energy storage/conversion and sensor, J. Energy Storage 83 (2024) 110650.
[148] J. Pang, J. Li, J. Guo, M. Jia, J. Zhang, Tuning the aggregation structure and surface composition of reduced graphene oxide microspheres for high-rate supercapacitors, Diam. Relat. Mater. 136 (2023) 109920.
[149] S. Bykkam, D.N. Prasad, M.R. Maurya, K.K. Sadasivuni, J.-J. Cabibihan, Comparison study of metal oxides (CeO_2, CuO, SnO_2, CdO, ZnO and TiO_2) decked few layered graphene nanocomposites for dye-sensitized solar cells, Sustainability 13 (2021) 7685.
[150] N.P.D. Ngidi, E. Muchuweni, V.O. Nyamori, Synthesis and characterisation of heteroatom-doped reduced graphene oxide/bismuth oxide nanocomposites and their application as photoanodes in DSSCs, RSC Adv. 12 (2022) 2462–2472.
[151] A. Alshahrie, A.A. Alghamdi, P.M.Z. Hasan, F. Ahmed, H.M.E. Albalawi, A. Umar, A. Alsulami, Enhancement in the performance of dye sensitized solar cells (DSSCs) by incorporation of reduced graphene oxide (RGO) and carbon nanotubes (CNTs) in ZnO nanostructures, Inorganics 10 (2022) 204.
[152] X. Atanacio-Sánchez, W.J. Pech-Rodríguez, E.N. Armendáriz-Mireles, J. A. Castillo-Robles, P.C. Meléndez-González, E. Rocha-Rangel, Improving performance of ZnO flexible dye sensitized solar cell by incorporation of graphene oxide, Microsyst. Technol. 26 (2020) 3591–3599.
[153] S. Sha, H. Lu, S. Yang, T. Li, J. Wu, J. Ma, K. Wang, C. Hou, Z. Sheng, Y. Li, One-step electrodeposition of ZnO/graphene composite film as photoanode for dye-sensitised solar cells, Colloids Surf. A: Physicochem. Eng. Asp. 630 (2021) 127491.
[154] H. Abdullah, S. Mahalingam, N.A. Abu Bakar, A. Manap, M.H.D. Othman, M. Akhtaruzzaman, Influence of Fe_2O_3 in ZnO/GO-based dye-sensitized solar cell, Polym. Bull. 79 (2022) 4287–4301.
[155] R. Savari, J. Rouhi, O. Fakhar, S. Kakooei, D. Pourzadeh, O. Jahanbakhsh, S. Shojaei, Development of photo-anodes based on strontium doped zinc oxide-reduced graphene oxide nanocomposites for improving performance of dye-sensitized solar cells, Ceram. Int. 47 (2021) 31927–31939.
[156] K.K. Saravanan, P. SivaKarthik, Ru-dye grafted CuS and reduced graphene oxide (CuS/rGO) composite: an efficient and photo tunable electrode for dye sensitized solar cells, J. Clust. Sci. 31 (2020) 401–407.
[157] D. Krishnamoorthy, A. Prakasam, Preparation of MoS_2/graphene nanocomposite-based photoanode for dye-sensitized solar cells (DSSCs), Inorg. Chem. Commun. 118 (2020) 108016.
[158] D. Krishnamoorthy, A. Prakasam, Graphene hybridized with tungsten disulfide (WS_2) based heterojunctions photoanode materials for high performance dye sensitized solar cell device (DSSCs) applications, J. Clust. Sci. 32 (2021) 621–630.
[159] R. Sasikala, M. Kandasamy, V. Ragavendran, S. Suresh, V. Sasirekha, S. Murugesan, S. Sagadevan, J. Mayandi, Perovskite zinc titanate-reduced graphene oxide nanocomposite photoanode for improved photovoltaic performance in dye-sensitized solar cell, Phys. B: Condens. Matter 646 (2022) 414300.
[160] R. Sasikala, M. Kandasamy, S. Suresh, V. Ragavendran, V. Sasirekha, N. Pugazhenthiran, S. Murugesan, S.A. Pandian, M.N.M. Ansari, J. Mayandi, Strontium titanate perovskite embedded reduced graphene oxide photoanode for dye-sensitized solar cell, Opt. Mater. 136 (2023) 113464.
[161] S.A. Pandian, M. Sivakumar, M. Kandasamy, S. Suresh, G.M. Latha, S. Srinivasan, K.P. Ananth, Barium titanate nanorods/nanoparticles embedded reduced graphene oxide nanocomposite photoanode for dye-sensitized solar cell, Chem. Phys. Lett. 851 (2024) 141491.
[162] S.A. Pandian, M. Sivakumar, Hoisting photovoltaic performance of perovskite $BaSnO_3$ nanoparticles wrapped reduced graphene oxide: efficient photoelectrode for dye-sensitized solar cell, Mater. Today.: Proc. (2023), https://doi.org/10.1016/j.matpr.2023.01.415.
[163] S. Ndlovu, E. Muchuweni, M.A. Ollengo, V.O. Nyamori, Tuning the properties of reduced graphene oxide-$Sr_{0.7}Sm_{0.3}Fe_{0.4}Co_{0.6}O_3$ nanocomposites as potential photoanodes for dye-sensitized solar cells, J. Electron. Mater. 52 (2023) 5843–5860.
[164] H.G. Lemos, D. Barba, G.S. Selopal, C. Wang, Z.M. Wang, A. Duong, F. Rosei, S. F. Santos, E.C. Venancio, Water-dispersible polyaniline/graphene oxide counter electrodes for dye-sensitized solar cells: Influence of synthesis route on the device performance, Sol. Energy 207 (2020) 1202–1213.
[165] O. Omelianovych, L.L. Larina, H.-J. Oh, E. Park, V.-D. Dao, H.-S. Choi, Plasma-processed CoSn/RGO nanocomposite: a low-cost and sustainable counter electrode for dye-sensitized solar cells, Sol. Energy 201 (2020) 819–826.
[166] A.A. Oladipo, M. Gazi, Ternary $Ni_{0.5}Zn_{0.5}Fe_2O_4$/carbon nanocomposite as counter electrode for natural dye-sensitized solar cells: electro-photovoltaic characterizations, J. Photochem. Photobiol. A: Chem. 425 (2022) 113665.
[167] P. Gemeiner, M. Pavličková, M. Hatala, M. Hvojnik, T. Homola, M. Mikula, The effect of secondary dopants on screen-printed PEDOT:PSS counter-electrodes for dye-sensitized solar cells, J. Appl. Polym. Sci. 139 (2022) 51929.
[168] V. Saranya, S. Athithya, S. Muthu Mariappan, M. Navaneethan, J. Archana, Unravelling the catalytic activity of copper cobalt oxide - nickel cobalt oxide composites for efficient counter electrode performance in DSSCs, J. Alloy. Compd. 988 (2024) 173993.
[169] A.F. Abdelaal, M. Younas, R.N. Iman, A. Damdam, A.M. Al-Amri, T.N. Baroud, Fabrication of efficient and economical dye-sensitized solar cells using carbon-coated nanotextured silicon wafers counter electrodes, Synth. Met. 301 (2024) 117537.
[170] S.H. Bendary, A.A. Abdelrahman, Flexible and novel counter electrode from graphene/Zn Al layered double hydroxide nanocomposite in dye sensitized solar cells, J. Electroanal. Chem. 922 (2022) 116736.
[171] K. Gomathi, S. Padmanathan, A.M. Ali, A.T. Rajamanickam, Construction of Ni doped MoO_3 nanostructures and their application as counter electrode in dye-sensitized solar cells, Inorg. Chem. Commun. 135 (2022) 109079.
[172] A. Alizadeh, M. Roudgar-Amoli, Z. Shariatinia, E. Abedini, S. Asghar, S. Imani, Recent developments of perovskites oxides and spinel materials as platinum-free counter electrodes for dye-sensitized solar cells: a comprehensive review, Renew. Sustain. Energy Rev. 187 (2023) 113770.
[173] B. Palanivel, B.A. Kumar, R. Gopal, F.H. Alkallas, M. Shkir, S. AlFaify, Surfactant assisted $FeCo_2O_4$ nanostructure: an efficient counter electrode for dye sensitized solar cell assisted hexagonal and photocatalyst for dye degradation, Optik 280 (2023) 170786.
[174] K.-L. Teng, X.-Y. Lin, S.-H. Liu, Y.-H. Yu, C.-H. Tsai, B.-X. Yang, S.-Y. Chien, Nitrogen, sulfur coordinated metal complex and reduced graphene oxide hybrid materials as counter electrodes for application in dye-sensitized solar cells, Org. Electron. 125 (2024) 106977.
[175] J. Qian, Q. Lu, F. Xu, G. He, J. Xia, Fabrication of three-dimentional triarylmethane polymers derivatives as efficient counter electrodes for dye-sensitized solar cells, Electrochim. Acta 408 (2022) 139917.
[176] M.S. Ahmad, A.K. Pandey, N.A. Rahim, N. Aslfattahi, Y.K. Mishra, B. Rashid, R. Saidur, 2-D Mxene flakes as potential replacement for both TCO and Pt layers for dye-sensitized solar cell, Ceram. Int. 47 (2021) 27942–27947.
[177] Y. Yuan, C. Wan, Dual application of waste grape skin for photosensitizers and counter electrodes of dye-sensitized solar cells, Nanomaterials 12 (2022) 563.
[178] S. Gnanasekar, A. Nirmala Grace, V_2O_5 nanosheets as an efficient, low-cost Pt-free alternate counter electrode for dye-sensitized solar cells, ChemNanoMat 8 (2022) e202100382.
[179] L.V. Cuong, N.D. Thinh, L.T.T. Nghia, N.D. Khoa, L.K. Hung, H.H. Dat, P.T. Khang, N.T. Hoang, P.T.L. Chau, M.T. Phong, N.H. Hieu, Synthesis of platinum/reduced graphene oxide composite pastes for fabrication of cathodes in dye-sensitized solar cells with screen-printing technology, Inorg. Chem. Commun. 118 (2020) 108033.
[180] A.-F. Kanta, A. Decroly, Stainless steel electrode characterizations by electrochemical impedance spectroscopy for dye-sensitized solar cells, Electrochim. Acta 56 (2011) 10276–10282.
[181] T.N. Murakami, M. Grätzel, Counter electrodes for DSC: application of functional materials as catalysts, Inorg. Chim. Acta 361 (2008) 572–580.
[182] J.S. Choi, H.B. Park, O.J. Yoon, H.J. Kim, Investigation on the role of graphene oxide sheet-platinum composite counter electrode in dye-sensitized solar cell, Thin Solid Films 745 (2022) 139098.
[183] S. Venkatesan, D. Manurung, H. Teng, Y.-L. Lee, Efficiency and stability improvements for room light dye-sensitized solar cells in the presence of electrochemically fabricated composite counter electrodes, J. Power Sources 518 (2022) 230781.
[184] S. Mohammadnejad, M.R. Mohammadi, H.M. Ghartavol, M. Askari, Lithium-functionalized graphene oxide with a low load of Pt as an efficient counter electrode for dye-sensitized solar cells, J. Appl. Electrochem. 54 (2024) 275–287.
[185] A. Asok, K. Haribabu, Synthesis and performance of polythiophene-iridium oxide composite as counter electrode in dye sensitized solar cell, Curr. Appl. Phys. 49 (2023) 64–69.
[186] X. Zhang, X. Wang, Y. Cao, C. Liang, S. Geng, H. Guo, Y. Liu, Y. Luo, W. Zhang, L. Li, Facile synthesis of $ZnCo_2O_4$@$NiMoO_4$ with porous coated structures on carbon paper as stable and efficient Pt-free counter electrode materials for advanced dye-sensitized solar cells, Appl. Surf. Sci. 616 (2023) 156461.
[187] A. Agrawal, S.A. Siddiqui, A. Soni, G.D. Sharma, Advancements, frontiers and analysis of metal oxide semiconductor, dye, electrolyte and counter electrode of dye sensitized solar cell, Sol. Energy 233 (2022) 378–407.
[188] S.E. Sheela, R. Sekar, D.K. Maurya, M. Paulraj, S. Angaiah, Progress in transition metal chalcogenides-based counter electrode materials for dye-sensitized solar cells, Mater. Sci. Semicond. Process. 156 (2023) 107273.
[189] M. Mirzaei, M.B. Gholivand, Core-shell structured $Ni_{0.85}Se$@MoS_2 nanosheets anchored on multi-walled carbon nanotubes-based counter electrode for dye-sensitized solar cells, Electrochim. Acta 432 (2022) 141179.
[190] M. Ayaz, M. Hijji, A.S. Alatawi, M.A. Namazi, M.I.M. Ershath, Enhancing photovoltaic performance in dye-sensitized solar cells using nanostructured NiS/MoS_2 composite counter electrodes, Mater. Sci. Semicond. Process. 173 (2024) 108172.

[191] W.-C. Oh, Y. Liu, Y. Areerob, A novel fabrication of organic-inorganic hybridized Graphene-La_2CrFeW_6 nanocomposite and its improved photovoltaic performance in DSSCs, J. Sci.: Adv. Mater. Devices 6 (2021) 271–279.
[192] A.A. Qureshi, S. Javed, H.M.A. Javed, A. Akram, M. Jamshaid, A. Shaheen, Strategic design of Cu/TiO_2-based photoanode and rGO-Fe_3O_4-based counter electrode for optimized plasmonic dye-sensitized solar cells, Opt. Mater. 109 (2020) 110267.
[193] R. Senthilkumar, S. Ramakrishnan, M. Balu, S.K. Batabyal, D.J. Yoo, D. Kumaresan, N.K. Kothurkar, $Co_xMo_{(1-x)}S_2$ intermixed reduced graphene oxide as efficient counter electrode materials for high-performance dye-sensitized solar cells, Int. J. Hydrog. Energy 48 (2023) 5901–5914.
[194] K. Silambarasan, J. Archana, S. Athithya, S. Harish, R.S. Ganesh, M. Navaneethan, S. Ponnusamy, C. Muthamizhchelvan, K. Hara, Y. Hayakawa, Hierarchical NiO@NiS@graphene nanocomposite as a sustainable counter electrode for Pt free dye-sensitized solar cell, Appl. Surf. Sci. 501 (2020) 144010.
[195] C. Zou, M. Chen, Z. Zhou, S. Yang, Y. Hou, H. Yang, Highly ordered mesoporous Co_3O_4 cubes/graphene oxide heterostructure as efficient counter electrodes in dye-sensitized solar cells, J. Mater. Sci.: Mater. Electron. 32 (2021) 16519–16527.
[196] L. Sun, Q. Zhang, Q. Liang, W. Li, X. Li, S. Liu, J. Shuai, α-Fe_2O_3/reduced graphene oxide composites as cost-effective counter electrode for dye-sensitized solar cells, Catalysts 12 (2022) 645.
[197] P.J.S. Jennifer, S. Muthupandi, M.J.R. Ruban, S. Prathap, J. Madhavan, M.V. A. Raj, A quaternary nanocomposite as an efficient counter electrode for Pt-free Dye-sensitized solar cells (DSSC), Mater. Lett. 340 (2023) 134151.
[198] W.C. Oh, K.Y. Cho, C.H. Jung, Y. Areerob, Hybrid of graphene based on quaternary $Cu_2ZnNiSe_4$-WO_3 nanorods for counter electrode in dye-sensitized solar cell application, Sci. Rep. 10 (2020) 4738.
[199] C. Tamilselvi, P. Duraisamy, N. Subathra, Graphene wrapped $NiSe_2$ nanocomposite-based counter electrode for dye-sensitized solar cells (DSSCs), Diam. Relat. Mater. 116 (2021) 108396.
[200] P. Wei, Z. Hao, Y. Yang, L. Liu, Hollow $NiSe_2$ nanospheres grown on graphene with unconventional dual-vacancies in dye-sensitized solar cells, Appl. Surf. Sci. 553 (2021) 149567.
[201] S. Wang, Y. Xie, K. Shi, W. Zhou, Z. Xing, K. Pan, A. Cabot, Monodispersed nickel phosphide nanocrystals in situ grown on reduced graphene oxide with controllable size and composition as a counter electrode for dye-sensitized solar cells, ACS Sustain. Chem. Eng. 8 (2020) 5920–5926.
[202] S. Kumar, N. Kaur, V. Bhullar, A. Mahajan, MoS_2 nanorods anchored reduced graphene oxide nanohybrids for electrochemical energy conversion applications, Phys. E: Low. -Dimens. Syst. Nanostruct. 128 (2021) 114589.
[203] L. Yi, H. Sun, W. Yang, W. Chen, J. Luo, J. Wang, X. Kang, D. Luo, B. Ma, Y. Wang, S. Su, Z. Wang, Study of microwave-assisted MoS_2 and graphene composite counter electrode for dye-sensitized solar cells, Front. Mater. 8 (2021) 644432.
[204] K. Silambarasan, S. Harish, K. Hara, J. Archana, M. Navaneethan, Ultrathin layered MoS_2 and N-doped graphene quantum dots (N-GQDs) anchored reduced graphene oxide (rGO) nanocomposite-based counter electrode for dye-sensitized solar cells, Carbon 181 (2021) 107–117.
[205] W. Mao, L. Wei, X. Xu, L. Zhao, J. Liu, Z. Zhang, One-step hydrothermal preparation of bi-functional NiS_2/reduced graphene oxide composite electrode material for dye-sensitized solar cells and supercapacitors, Int. J. Hydrog. Energy 48 (2023) 28377–28389.
[206] A. Sarkar, S. Bera, A.K. Chakraborty, $CoNi_2S_4$-reduced graphene oxide nanohybrid: an excellent counter electrode for Pt-free DSSC, Sol. Energy 208 (2020) 139–149.
[207] G. Sankar, P. Anbarasu, R. Mahendran, K. Rajendran, T. Sivakumar, Pt-free and efficient counter electrode with nanostructured $CoNi_2S_4$/rGO for dye-sensitized solar cells, Inorg. Chem. Commun. 126 (2021) 108475.
[208] G. Sankar, P. Anbarasu, R. Mahendran, K. Sambath, K. Prammapriya, Design and fabrication of Pt-free $FeNi_2S_4$/rGO hybrid composite thin films counter electrode for high-performance dye-sensitized solar cells, J. Mater. Sci.: Mater. Electron. 32 (2021) 11910–11920.
[209] S. Ndlovu, E. Muchuweni, M.A. Ollengo, V.O. Nyamori, Highly efficient nitrogen-doped reduced graphene oxide-$Sr_{0.7}Sm_{0.3}Fe_{0.4}Co_{0.6}O_{2.65}$ nanocomposites utilized as a counter electrode in dye-sensitized solar cells, Mater. Today Commun. 38 (2024) 107681.